JOURNAL OF PETROLOGY | VOLUME 55 | NUMBER 6 | PAGES 1051–1082 | 2014 | doi:10.1093/petrology/egu017

The Global Systematics of Ocean Ridge Basalts and their Origin

ALLISON GALE[1,2]*, CHARLES H. LANGMUIR[1] AND COLLEEN A. DALTON[3]

[1]DEPARTMENT OF EARTH AND PLANETARY SCIENCES, HARVARD UNIVERSITY, 20 OXFORD ST., CAMBRIDGE, MA 02138, USA

[2]DEPARTMENT OF PLANT AND EARTH SCIENCE, UNIVERSITY OF WISCONSIN, RIVER FALLS, 410 S. 3RD ST., RIVER FALLS, WI 54022, USA

[3]DEPARTMENT OF GEOLOGICAL SCIENCES, BROWN UNIVERSITY, 324 BROOK ST., PROVIDENCE, RI 02912, USA

RECEIVED AUGUST 14, 2013; ACCEPTED MARCH 24, 2014

Tests of models of melt generation and mantle source variations beneath mid-ocean ridges require a definitive set of mid-ocean ridge basalt (MORB) compositions corrected for shallow-level processes. Here we provide such a dataset, with both single sample and segment means for 241 segments from every ocean basin, which span the entire range of spreading rate, axial depth, and MORB chemical composition. Particular attention is paid to methods of fractionation correction. Values corrected to 8 wt % MgO are robust as they are within the range of the data. Extrapolation to equilibrium with mantle olivine is a non-unique procedure that is critically dependent on the MgO content where plagioclase first appears. MORB data, trace element ratios and calculated liquid lines of descent provide consistent evidence that plagioclase fractionation primarily occurs between 8 and 9 wt % MgO, with the exception of hydrous magmas mainly from back-arc segments. Varying the MgO content of plagioclase appearance over large ranges does not produce the observed systematics at 8 wt % MgO, but may contribute to the spread of the data. Data were evaluated individually for each segment to ensure reliable fractionation correction, and segment means are reported normalized both to MgO of 8 wt % and also to a constant Mg/(Mg + Fe) in equilibrium with Fo_{90} olivine. Both sets of corrected compositions show large variations in Na_2O and FeO, good correlations with segment depth, and systematic relationships among the major elements. A particularly good correlation exists between Al_{90} and Fe_{90}. These new data are not in agreement with the presentation of Niu & O'Hara (Journal of Petrology 49, 633–664, 2008), whose results relied on an inaccurate fractionation correction procedure, which led them to large errors for high- and low-FeO magmas. The entire dataset is provided in both raw and normalized form so as to have a uniform basis for future evaluations. The new data compilation permits tests of competing models for the primary causes of variations in MORB parental magmas: variations in mantle composition, mantle temperature, reactive crystallization or lithospheric thickness. The principal component of chemical variation among segment mean compositions is remarkably consistent with variations in mantle temperature of some 200°C beneath global ocean ridges. Comparisons with experimental data, pMELTS and other calculations show that variations in mantle fertility at constant mantle potential temperature produce trends that are largely orthogonal to the observations. At the same time, there is clear evidence for mantle major element heterogeneity beneath and around some hotspots and beneath back-arc basins. Super slow-spreading ridges display a characteristic chemical signature of elevated Na_{90} and Al_{90} and lowered Si_{90} relative to faster-spreading ridges. If this signature were produced by reactive crystallization, Si_{90} should be higher rather than lower in these environments owing to the thicker lithosphere and lower temperatures of mantle–melt reaction. Instead, the data are consistent with lower extents of mantle melting beneath a thicker lithosphere. Hence, variations in extent of melting appear to be the dominant control on the major element compositions of MORB parental magmas. Trace elements, in contrast, require a large component of mantle heterogeneity, apparent in the factor of 50 variation in K_{90}. Such variations do not correlate with the other major elements, showing that major element and trace

* Corresponding author. E-mail: agale23@gmail.com

element (and isotope) heterogeneity reflect different processes. This supports the model of movement of low-degree melts for the creation of trace element and isotope mantle heterogeneity, and is inconsistent with large variations in the amount of recycled crust in most ocean ridge mantle sources.

KEY WORDS: *geochemistry; major element; MORB; crust*

INTRODUCTION

Variations in the temperature and composition of the upper mantle have implications for mantle convection, volcanism, crustal uplift and subsidence, the range and origin of mantle compositional variability, and mantle evolution through time. The petrology of mid-ocean ridge basalts (MORB) provides a means to investigate these variations, as MORB are products of mantle melting and occur globally.

The potential temperature of the mantle must exert an influence on the overall extent of melting as the mantle ascends beneath ocean ridges. Hotter mantle intersects the solidus deeper, melting to a larger overall extent and producing a thicker basaltic crust. After isostatic adjustment, thicker crust will be at higher elevations than thinner crust, both because of the thicker crust and also because of elevated mantle temperatures and greater extents of melt depletion in the mantle (Klein & Langmuir, 1987). The concentrations of moderately incompatible elements, such as Na and Ti, vary approximately inversely with the extent of melting and are less influenced by mantle heterogeneity than highly incompatible elements. For a nearly homogeneous source, ridges with shallow depths should have lower concentrations of such elements, as shown to be the case by Klein & Langmuir (1987). They and Langmuir *et al.* (1992) interpreted global basalt chemical systematics in terms of mantle temperature variations of ~220°C, with the proviso that certain regions, such as ridges near the Azores and Galapagos hotspots, also required an important influence of mantle heterogeneity.

Such an interpretation, however, is by no means universally accepted, and is contradicted by geological evidence in some regions (Zhou & Dick, 2013). Some have argued that the temperature of the mantle is roughly uniform beneath ridges (e.g. Shen & Forsyth, 1995; Green *et al.*, 2001; Presnall *et al.*, 2002). Shen & Forsyth (1995), for example, called upon variations in the thickness of the oceanic lithosphere coupled with mantle heterogeneity to account for the chemical data. Others have asserted that compositional rather than temperature variations are the dominant effect on the chemical compositions of erupted basalts (e.g. Niu & O'Hara, 2008), and that variations in ridge depth are largely the result of mantle composition, with deep ridges underlain by denser, more fertile mantle. Still others have contended that melt–rock reaction can explain the global variations in mid-ocean ridge basalts (Kimura & Sano, 2012). Zhou & Dick (2013) recently provided geological evidence that the crust cannot be thick beneath shallow portions of the Southwest Indian Ridge, and suggested that depleted mantle leads to shallow ridge depths, at least in this region where thick crust is not viable. Even the global chemical systematics of MORB have been called into question, by making alternative corrections for low-pressure cooling and fractionation (Niu & O'Hara, 2008; Till *et al.*, 2012). Despite 25 years of additional data after the Klein & Langmuir (1987) study, persistent questions remain over the actual systematics of MORB compositions and the relative importance of mantle temperature, mantle composition and chemical changes during magma transport.

A first step towards clarifying these issues is a uniform and comprehensive global database with consistent fractionation corrections that can be used for the evaluation of various hypotheses. This study has as its first aim to utilize an unparalleled major element database in terms of size and quality (Gale *et al.*, 2013*a*), and an updated approach to fractionation correction, to arrive at estimates of mean parental magma composition for over 240 global ridge segments (Fig. 1). Careful evaluation when correcting for fractionation processes is essential to constrain variations in parental magmas. These data can then be used to test competing hypotheses for variations in ocean ridge depth and crustal composition, and to begin to explore the diversity of processes that produce the complexity of MORB worldwide.

DATA TREATMENT

The data used here are from the study by Gale *et al.* (2013*a*), where a compiled database of inter-laboratory bias-corrected, filtered, renormalized major element data for whole-rocks and glasses was presented. Although many of the data came from PetDB (Lehnert *et al.*, 2000), the database also included an extra ~1800 previously unpublished analyses. In addition to the new data, key differences in this compilation compared with a download of data from PetDB are the restriction of data to on-axis locations, inter-laboratory bias corrections, and manual checking of discrepancies with original publications. Perhaps most importantly, each sample with a major element analysis was also assigned to a unique ridge segment [catalog of ridge segments provided by Gale *et al.* (2013*a*)], providing the possibility of data normalization that is specific to particular locations and spreading rates, and permitting the calculation of robust segment averages.

Ridge segments were defined using GeoMapApp (Ryan *et al.*, 2009), and bathymetric profiles along-axis for each segment were determined with evenly spaced (~0·5 km, although it is regionally variable) points of latitude, longitude and elevation. 'Mean depth' for every segment is then

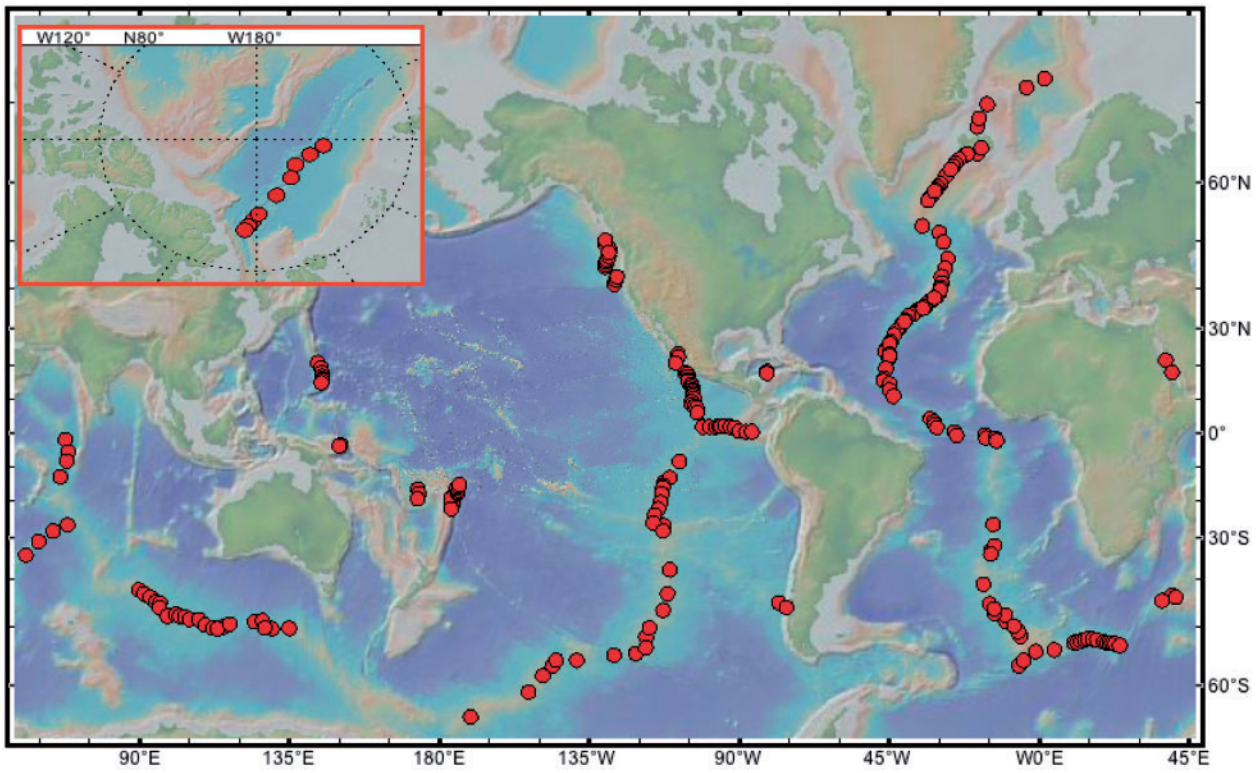

Fig. 1. Map showing the locations of segments with 8- and 90-values calculated in this study (circles). Inset shows the location of samples from the Gakkel Ridge in the Arctic. The new dataset includes data from the full range of spreading rates and ridge depths, and back-arc basins, and it excludes off-axis samples. Bathymetry from GeoMapApp (Ryan *et al.*, 2009).

defined as an average of the evenly spaced elevations. For 692 of the 771 ridge segments in the catalog, spreading rate was calculated at the midpoint of each segment using the rotation poles and angular velocities from NUVEL-1A (DeMets *et al.*, 1994) and the equations for relative motion on a plate boundary (e.g. Fowler, 2008). Spreading rates for back-arc spreading centers and for the Juan de Fuca Ridge were calculated from NR-MORVEL56 (Argus *et al.*, 2011), which includes the plate motions of 31 additional small plates defined by Bird (2003). The complete dataset is provided here as Supplementary Data (available for downloading at http://www.petrology.oxfordjournals.org) and discussion of the database procedures has been given by Gale *et al.* (2013*a*).

Data normalization to common MgO and Mg#

To evaluate mantle processes, it is necessary to take into account the chemical changes produced during transport of magmas from the mantle to the seafloor. MgO is a useful proxy for such changes, because it correlates well with temperature, and most other elements vary regularly with MgO. Basalts recovered from a single ridge segment can vary by more than 4 wt % in MgO content, with concomitant changes of ~6 wt % FeO and ~1·3 wt % Na_2O, about the same magnitude as the global range in FeO and Na_2O corrected to a single value of MgO (Klein & Langmuir, 1987). Multiple processes can cause variations in MgO, including crystallization and removal of crystals, magma mixing and reactions in crystal mushes. Whatever the process, correction of the data to a common MgO value is necessary to remove this low-pressure contribution to the chemical variation so as to determine a signal presumably dominated by mantle processes.

For closed-system crystallization, such corrections are well constrained within the range of natural basalt data. The chemical changes that accompany low-pressure crystallization of basaltic liquids are called 'liquid lines of descent' (LLD), or the path through compositional space traversed by a liquid during cooling. LLD for MORB are well documented by an abundance of experimental data (e.g. Tormey *et al.*, 1987; Grove *et al.*, 1992; Yang *et al.*, 1996), and can be modeled with LLD programs (e.g. Weaver & Langmuir, 1990; Danyushevsky & Plechov, 2011), which match observations well. The slopes of LLD are influenced by the temperature and composition at which a new phase appears. Plagioclase appearance, for example, has a strong effect on oxides such as FeO and Al_2O_3. The MgO content at which plagioclase appears is sensitive to the amount of H_2O in the magma, and clinopyroxene

appearance is strongly pressure-dependent. These effects can be dealt with, as water content can be measured and pressure estimated, and tested using the LLD programs. The agreement between observations, theory and experiments makes the closed-system problem well constrained. As long as one stays within the range of observed compositions, equilibria can be calculated and corrections accurately applied. Because most ridge segments span 8 wt % MgO, correction to this value permits correction without extrapolation, as it intersects the observations (Klein & Langmuir, 1987).

Although closed-system crystallization is a useful model that corresponds to many of the data, the petrography of MORB shows that closed-system crystallization is an oversimplification of the actual processes that take place (e.g. Dungan & Rhodes, 1978). Multiple generations of phenocrysts, mineral compositions that are out of equilibrium with the liquid, and evidence for magma mixing demonstrate that the actual processes must be more complex. Some researchers (O'Hara, 1977; O'Neill & Jenner, 2012) have asserted that multiple generations of mixing events can lead to substantial changes in apparent LLD. Langmuir & Hanson (1980) and Langmuir (1989) demonstrated that periodically replenished magma chambers are limited to mixing between fractional and equilibrium LLD, and that steady-state compositions with small amounts of replenishment and eruption are forced to the equilibrium LLD. Nonetheless, other complex fractionation processes could lead to fractionated magma compositions dissimilar to closed-system crystallization (e.g. Langmuir, 1989).

Given the complexities in correcting for the low-pressure effects that modify basalt compositions, an alternative approach to avoid correction has been to use only the most primitive basalts from a segment (e.g. basalts with >9 wt % MgO). This approach is problematic, however, for multiple reasons. First, many segments do not contain such primitive compositions, so global representation would be poor. Second, such an approach has the implicit assumption that the highest MgO compositions encompass the range of MORB parental magmas and are the parents of lower MgO basalts. High-MgO basalts that are erupted, however, are not necessarily parental to the more common lower MgO compositions. In particular, there is a high-MgO magma type erupted periodically around the global system of ridges, a 'HiAl' magma (e.g. Eason & Sinton, 2006), characterized by exceptionally high Al_2O_3 contents, high MgO, low SiO_2 (e.g. 48 wt % SiO_2) and often very low TiO_2. Such samples rarely represent the parents of segment mean compositions [e.g. Fig. 2; see also Gale *et al.* (2013*b*)] but occur sporadically in certain segments, particularly on the margins of hotspots (Melson & O'Hearn, 1979; Langmuir & Bender, 1984; Eason & Sinton, 2006; Laubier *et al.*, 2012; Gale *et al.*, 2013*b*). Selecting for ocean ridge basalts with >9 wt % MgO leads to a disproportionately high number of HiAl basalts—a distinct and unusual magma series—in the dataset. In fact, complexities involving the petrogenesis of HiAl lavas have led to their exclusion in this study, despite their primitive nature (see Supplementary Data).

Another approach is to make even larger corrections to bring magmas back to higher temperatures (i.e. MgO higher than any erupted MORB). For example, an increasingly popular method is to correct compositions back to putative compositions that are in equilibrium with the upper mantle (e.g. Stolper & Newman, 1994; Niu & O'Hara, 2008). In this case one leaves the constrained world of observed compositions, and must make assumptions about what phases to add or procedures to follow to return to more primitive compositions. As noted by Till *et al.* (2012), such choices can have a great influence on interpretations of mantle processes, and as we show below, great care must be taken with this procedure so as not to introduce significant distortions of the data.

Despite these complexities, data normalization is necessary to eliminate chemical variations produced by low-pressure processes, and cannot be avoided by simply selecting for the highest MgO basalts. Corrected values are best constrained by remaining within the range of the data, where little to no correction is necessary. Such corrected compositions are nonetheless removed from mantle melt compositions. To be sure that the normalization process does not influence our conclusions, we provide here compositions normalized both to 8 wt % MgO, and to compositions in equilibrium with a mantle olivine of composition Forsterite 90 (Fo_{90}). A value of 8 wt % MgO has the advantage of being well constrained by the compositions observed at ridges. Fo_{90} has the appeal of being able to be directly compared with experiments on mantle melting. We first go through the various steps taken to correct to 8 wt % MgO ('8-values'). Then we consider the complexities and problems associated with correction to Fo_{90} ('90-values'), and develop the approach that leads to the best-constrained values. Both sets of values are presented in the Supplementary Data.

Data are normalized at the segment scale

One of the major considerations is at what scale the data should be grouped. Ideally, one might consider that fractionation correction should be applied only to a group of lavas related by one fractionation process. This is rarely possible, even in subaerial settings where chronological and stratigraphic constraints can be applied. Magmas come from different vents at different times, from plumbing systems that are poorly known. On fast-spreading ridges, some sections of ridge 10–15 km in length can produce magmas that appear to lie on a single LLD, but in others, diverse, unrelated magmas erupt within meters of each other. For example, from the earliest studies of

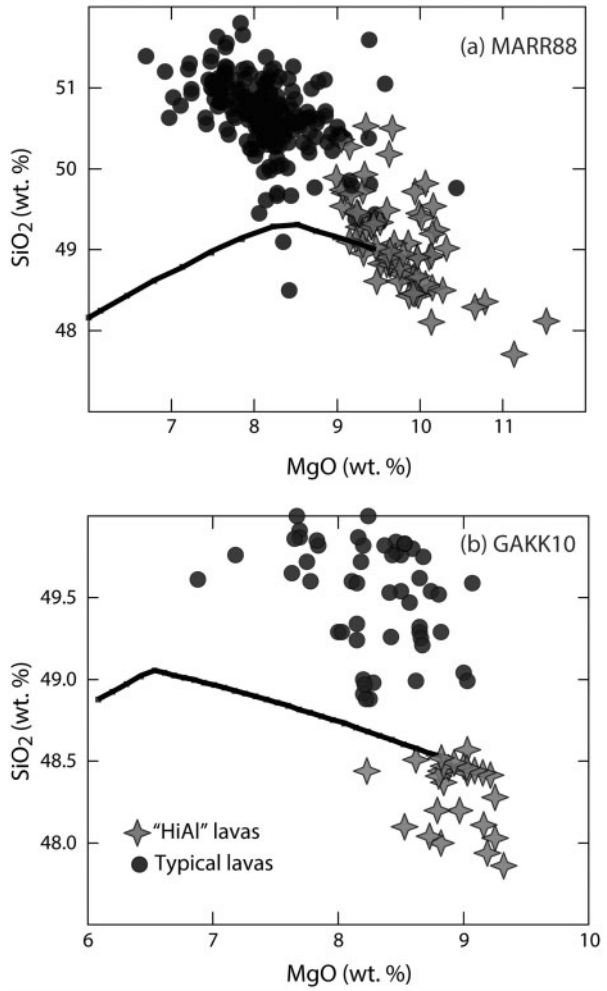

Fig. 2. Variation of SiO_2 vs MgO for segments MARR88 (a) and GAKK10 (b) demonstrating that 'HiAl' lavas—a particular magma type erupted periodically around the world marked by high MgO and Al_2O_3 and low SiO_2—cannot be parental to the typical lavas erupted at ridge segments. Continuous lines are liquid lines of descent (LLD) calculated from the HiAl lavas using hBasalt (Bezos *et al.*, in preparation). Olivine crystallizes alone initially, joined by plagioclase at about 8 wt % MgO, and then by clinopyroxene where the slope of the LLD becomes positive. The figure illustrates the point that a study of MORB that restricts itself to high-MgO lavas to avoid issues with fractionation correction inappropriately biases the study toward these distinct HiAl magmas, which are not parental melts to most MORB compositions.

slow-spreading ridges (e.g. Langmuir *et al.*, 1977; White & Bryan, 1977) it has been apparent that distinct parental magmas erupt within a single segment in close proximity. Even on the thin-section scale, analyses of melt inclusions show that multiple magmas contribute to erupted compositions (e.g. Laubier *et al.*, 2012, and references therein). For these reasons, a grouping based purely on samples simply related by low-pressure crystallization is not possible.

What is possible is the determination of average compositions on a segment scale. For comparisons with tectonic variables such as depth, and spreading rate, the 'ridge segment' is appropriate. Average depths for a total ridge segment remove the effects of potential buoyancy near the center and depression near segment ends. Whereas there may be multiple plumbing systems and parental magmas within a ridge segment, it is inevitable that there are separate plumbing systems in distinct segments; therefore petrological segmentation is ensured. Within each segment, although there are often diverse parental magmas, in most cases major element chemistry falls within limited ranges, and in any case errors on the means permit an evaluation of the magnitude of within-segment variability.

In this study we began with the 771 segments defined by Gale *et al.* (2013*a*) to group the petrological data and evaluate the processes and complexity that may be occurring at a given segment (Fig. 1). In rare cases, to avoid large gaps in global coverage, we grouped samples from two adjoining segments. For most segments, multiple parental magmas are required, and the segment average therefore represents a mean composition rather than a single parental composition that applies to all samples from the segment. Typically Na_2O varies by 0·5 wt % and FeO by 1·0–1·5 wt % at 8 wt % MgO where there are abundant samples (Fig. 3a–c). This is the 'local variation' discussed by Klein & Langmuir (1989) and Niu & Batiza (1994). Despite this diversity, the overall trend of most of the data is consistent with low-pressure LLD. In rare segments, the trend of the data is inconsistent with a single LLD, and even more diversity is present (Fig. 3d).

Segment-specific normalization to 8 wt % MgO

Owing to the observed chemical diversity, one procedure to normalize to 8 wt % MgO does not fit all segments, so each segment was independently evaluated for the optimal normalization parameters. The ability to customize the correction method improves the normalization, but does not control the overall characteristics of the normalized data. Corrected data generally have small errors (see Supplementary Data) and in most cases span 8 wt % MgO where no correction is applied. To ensure that the calculated 8-values are as free from bias as possible, all corrections were made prior to any plotting of the global segment chemical data or comparison with physical parameters such as ridge depth. All corrections were chosen and applied though an independent evaluation of each segment to try to obtain the most accurate representation of the data from that segment. Once the corrections were applied, no further changes were made (with the one exception of JUAN5).

For the normalization to be fully transparent and to allow for assessment by others, all diagrams and chosen regressions are available in the Supplementary Data for independent appraisal by interested readers. This material also provides many details on the specific correction

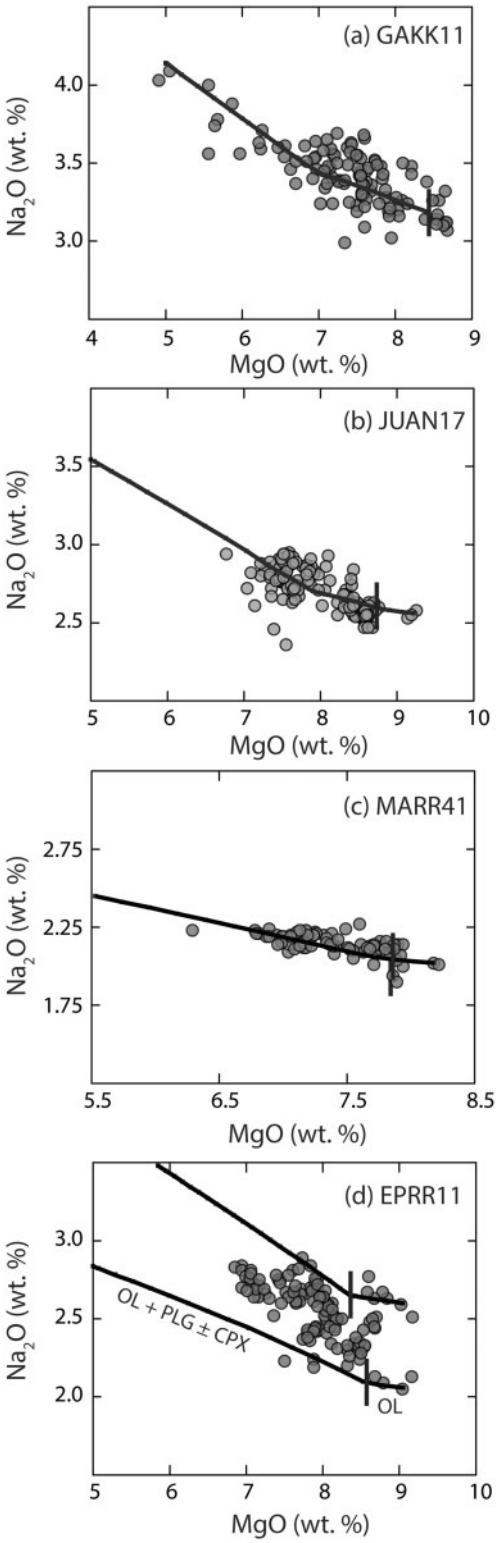

Fig. 3. Variation of Na_2O vs MgO for four representative mid-ocean ridge segments (a–d) including a high-Na_2O segment (GAKK11), medium-Na_2O segment (JUAN17), and a low-Na_2O segment (MARR41). It should be noted that in panels (a)–(c), calculated LLD (hBasalt; Bezos *et al.*, in preparation) track the data array closely despite the wide range of Na_2O contents for each segment. In these cases, the slopes used for correction to 8 wt % MgO can be understood as crystal fractionation control lines. Certain segments, however, such as EPRR11 (d), exhibit more variation within a segment than can be explained by simple crystal fractionation (e.g. Bender *et al.*, 1984). In such segments, the apparent slope of the data is not coincident with the estimated LLD slopes, implying the existence of multiple parental magmas. The tick mark on the indicated LLD is the boundary between the olivine-only slope and the olivine + plag ± cpx slope.

procedures utilized in this study for correction of basalts to 8 wt % MgO. All the variation diagrams are available in the Supplementary Data as well as the method code selection, the slope used, and the average and standard deviation of the segment 8-values. Also provided is a separate file including the individual glass samples with their major elements corrected to 8 wt % MgO that were included in the calculation of the mean segment 8-values, along with the original data for comparison. Customizing the correction to suit each ridge segment rather than applying a single formula to the entire dataset distinguishes this work from all previous studies. It also ensures that the 8-values correspond as closely as possible to the data distribution in each segment.

To arrive at a final segment 8-value, all samples with 8-values determined were averaged to determine a segment mean. A more accurate segment mean could include many other aspects, most of which are not practical for ridge segments. Knowledge of flow volume would permit a volumetric mean—but such information is not available for most segments. Instead, the assumption is that surface sampling provides a representative sample. There may also be hidden biases to such sampling—for example, seagoing scientists may prefer to target bathymetric bull's-eyes and cones rather than the lower relief areas. Segment-scale maps with flow thicknesses and hundreds of analyses would be ideal. Such data do not exist for any submarine ridge segment. Another consideration is that the mean we seek is the mean of parental magma compositions, and more fractionated magmas represent smaller portions of their original parent than more primitive compositions. One could then argue for a weighted mean based on MgO content. The presentation of the complete dataset permits others to investigate these and other possibilities.

The existence of careful studies of the subaerial Iceland segments allows one assessment of the viability of the presented means. Shorttle and Maclennan (2011) calculated volume-averaged segment means for Iceland, and these means compare well with those estimated here. At Iceland the segment-scale compositional range is large, and there are the additional complications of glaciation affecting melting. That the volume-averaged means of

Shorttle and Maclennan (2011) agree well with our segment means, in a region where the mismatch between simple means and volume-averaged means is likely to be large, adds confidence to the mean estimates here, but also may be fortuitous. Further assessments will be useful in coming years.

The data quantity and quality and the amount of 'geological noise' in different ridge segments is variable. Some segments have abundant data with clear and tight LLD. Others have few data and substantial scatter. Based on the appearance of the data, a 'confidence number' was assigned to the data from each segment, from 1 to 3, to give a sense of how well the 8-value could be estimated. These estimates are qualitative. Examples of segments corresponding to each confidence interval are shown in the Supplementary Data. Importantly, the main results are the same whether considering all segments or only the highest-confidence segments. The errors on the segment 8-values are generally small. This is illustrated in Fig. 4, which shows both raw data and 8-values for representative segments.

The fractionation and averaging methods presented above allow calculation of corrected values for 241 segments, which span all the ocean basins, the total range of axial depth from +1000 to −5400 m, and a range of spreading rates from <10 mm a^{-1} for the Gakkel Ridge to the superfast-spreading East Pacific Rise at 150 mm a^{-1} (Fig. 5). This coverage compares, for example, with the 84 data points that were used in the original Klein & Langmuir (1987) study. The new dataset, with triple the data coverage, inclusion of all the elements (e.g. Al_2O_3), more tightly constrained fractionation correction, far better geographical constraints, and correction for inter-laboratory bias, permits a rigorous and comprehensive re-evaluation of the global relationships of mid-ocean ridge basalts.

Figure 5 illustrates one of the predominant characteristics of the ocean ridge system: the standard deviation of most mantle-derived properties decreases with increasing spreading rate. This was originally suggested for radiogenic isotopes (e.g. Batiza, 1984), discussed at length by Langmuir *et al.* (1992), and is true for many physical and chemical characteristics of the ridge system. This conclusion appears to be in partial contradiction to the results of Rubin & Sinton (2007), who concurred that the standard deviation of mantle properties decreased with increasing spreading rate, but suggested that the standard deviation

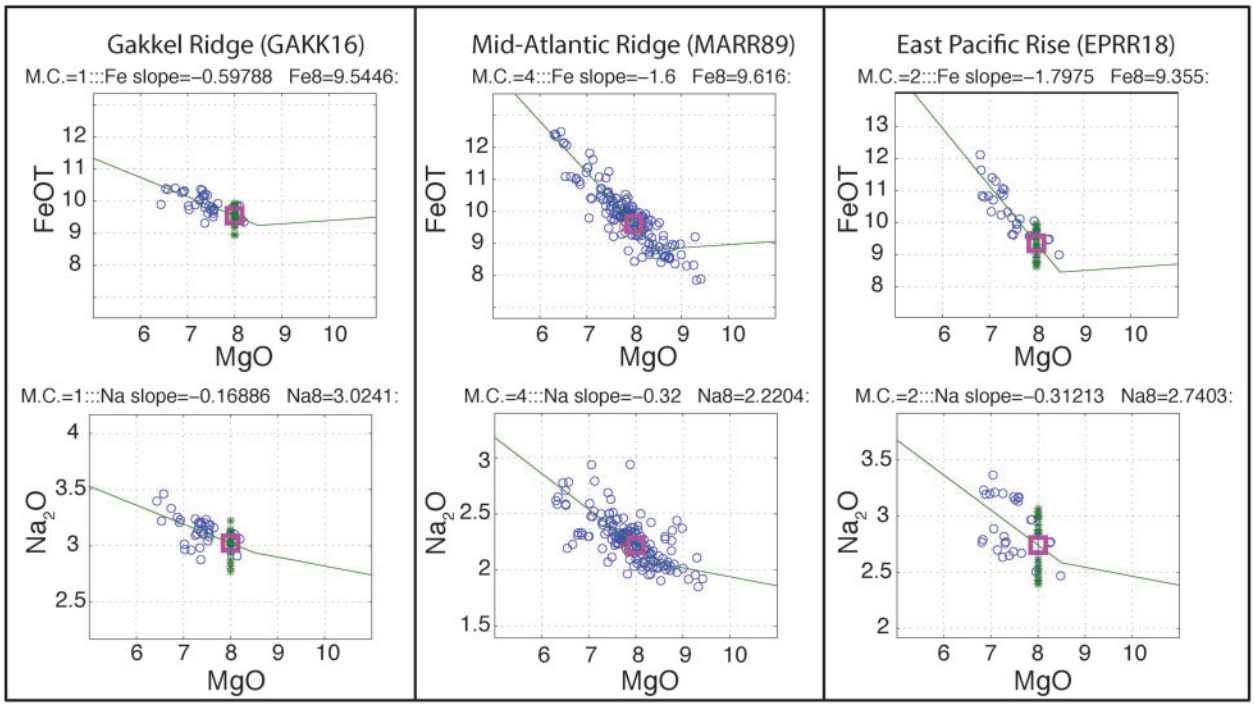

Fig. 4. Examples of variation diagrams (FeO vs MgO and Na_2O vs MgO) for three segments from the global catalog. Open circles indicate the sample data, lines show the slopes (olivine only and custom) used for correction to 8 wt % MgO, asterisks show the location of the corrected samples at 8 wt % MgO, and the box indicates the calculated mean segment '8-value'. Also shown at the top of each diagram are the custom slope value, the mean segment 8-value, and the method code (M.C.) used for calculating the 8-values (See Supplementary Data for details). It should be noted that from region to region there are variable, but well-constrained, fractionation slopes. The method used in this study accounts for this variation by allowing the data to define the slope for fractionation correction, as opposed to the 'constant-slope' and polynomial corrections found in the literature. It should be noted also that each mean segment 8-value is well constrained by the data. Similar diagrams for all segments are available in the Supplementary Data.

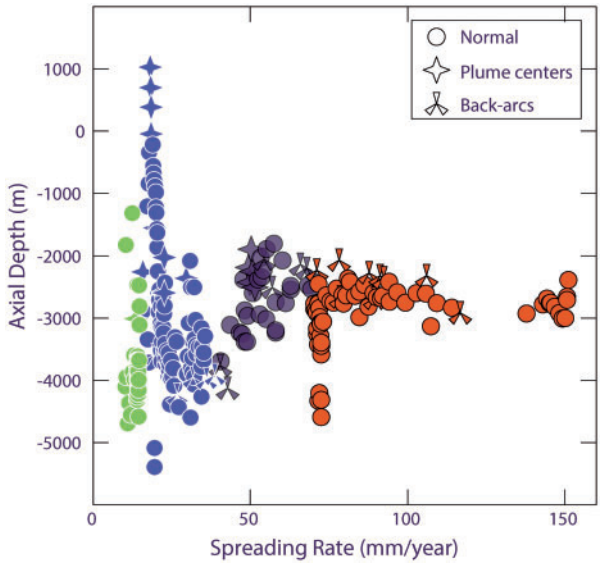

Fig. 5. Axial depth vs full spreading rate for the 241 ridge segments considered in this study. Color tones relate to spreading rate (four bins of different colours: bin 1, spreading rate >70 mm a^{-1}, bin 2, spreading between 40 and 70 mm a^{-1}, bin 3, spreading between 15 and 40 mm a^{-1}, bin 4, spreading <15 mm a^{-1}). 'Plume centers' are defined as any segment within 200 km of a hotspot. This study includes fractionation-corrected values from the full range of axial depths (+1000 to −5000 m) and spreading rates found along the length of the global mid-ocean ridge system. It should be noted that the standard deviation of depths increases with decreasing spreading rate.

of MgO contents at a given segment increased with increasing spreading rate. The latter conclusion was strongly influenced by the occurrence of highly fractionated andesites and dacites on fast-spreading ridges, and the exclusion of data from hotspot-influenced ridges, and is not pertinent to the discussion here. Their conclusion for mantle-derived properties is in agreement with the normalized data considered here, and parameters discussed previously (Batiza, 1984; Langmuir *et al.*, 1992).

Results at MgO = 8 wt %

Many of the chemical '8' parameters correlate to varying degrees with the average depth of the ridge segment (Fig. 6). Ridge segments near Iceland are all offset to shallower depths relative to correlations based on data from other regions. $Na_{8\cdot0}$ and $Al_{8\cdot0}$ correlate well with ridge depth. With the exception of back-arc basins (BAB), which are low in $Ti_{8\cdot0}$, and the subaerial Iceland segments, there is a crude positive correlation between $Ti_{8\cdot0}$ and depth. $Si_{8\cdot0}$ has a rough positive correlation with depth. $Fe_{8\cdot0}$ and $Ca_{8\cdot0}$ correlate negatively with depth. Shallow ridge segments are generally characterized by low Na_2O, low Al_2O_3, high FeO, low SiO_2, low TiO_2 and high CaO, and deep ridge segments are the opposite. These are the same systematics as identified by Klein & Langmuir (1987) and Langmuir *et al.* (1992), with the addition of Al_2O_3.

There are also relationships among the major element oxides (Fig. 7). $Na_{8\cdot0}$ correlates well (negatively) with $Ca_{8\cdot0}/Al_{8\cdot0}$, owing to a positive correlation with $Al_{8\cdot0}$ and negative correlation with $Ca_{8\cdot0}$. There is also a striking and strong negative correlation between $Fe_{8\cdot0}$ and $Al_{8\cdot0}$ (Fig. 7). A negative correlation also exists between $Na_{8\cdot0}$ and $Fe_{8\cdot0}$ for most ridge segments, with substantial offsets to low $Fe_{8\cdot0}$ for BAB basalts and many segments along the Mid-Atlantic Ridge (MAR) near the Azores plume (Langmuir *et al.*, 1992; Gale *et al.*, 2011). The co-variation between $Na_{8\cdot0}$ and $Ti_{8\cdot0}$ is complex. BAB have been shown to be offset to low $Ti_{8\cdot0}$ (e.g. Langmuir *et al.*, 2006*a*), clearly evident in this new compilation. The BAB as a group have a positive correlation between $Na_{8\cdot0}$ and $Ti_{8\cdot0}$. For open-ocean ridges the superslow-spreading ridges have high $Na_{8\cdot0}$ at the same $Ti_{8\cdot0}$ as other ridges.

There are no global correlations between $K_{8\cdot0}$ and other major element parameters. Mantle heterogeneity is almost invariably documented on the basis of radiogenic isotopes that are responsive to changes in highly incompatible element ratios and abundances, of which K_2O is the only representative among the 'major elements'. If mantle heterogeneity as documented by incompatible elements is caused by movements of large masses of mantle material that influence the mineral proportions and major element composition of the mantle, one might expect good correlations between $K_{8\cdot0}$ and the other major elements. At the same time, processes such as partial melting should also lead to good correlations between $K_{8\cdot0}$ and other major elements. Because these are not observed, it suggests that there are additional influences on $K_{8\cdot0}$ variations that can be produced without substantially changing other major element parameters. The variations in the segment means are also indicative of the substantial heterogeneity that can be observed in $K_{8\cdot0}$ for single samples from ridge segments. The variability of $K_{8\cdot0}$ within segments can be explored by considering the data and diagrams provided in the Supplementary Data.

Shown in the figures are the error bars for the data points calculated as two standard deviations of the mean for each segment. Although occasionally the errors are large relative to the size of the data points, particularly for ridge segments with few samples, it is clear that errors on segment averages are not the cause of the scatter and complex trends in the various diagrams. Instead, there are real variations that need to be accounted for, and deserve investigation in greater detail. No single process can account for the data distribution.

Comparison with early global studies

One of the purposes of the present study is to test whether the results of Klein & Langmuir (1987) and Langmuir *et al.* (1992), now over 20 years old, remain valid given the advances in data coverage and treatment. The tripling of data includes many regions of the global ridge system that

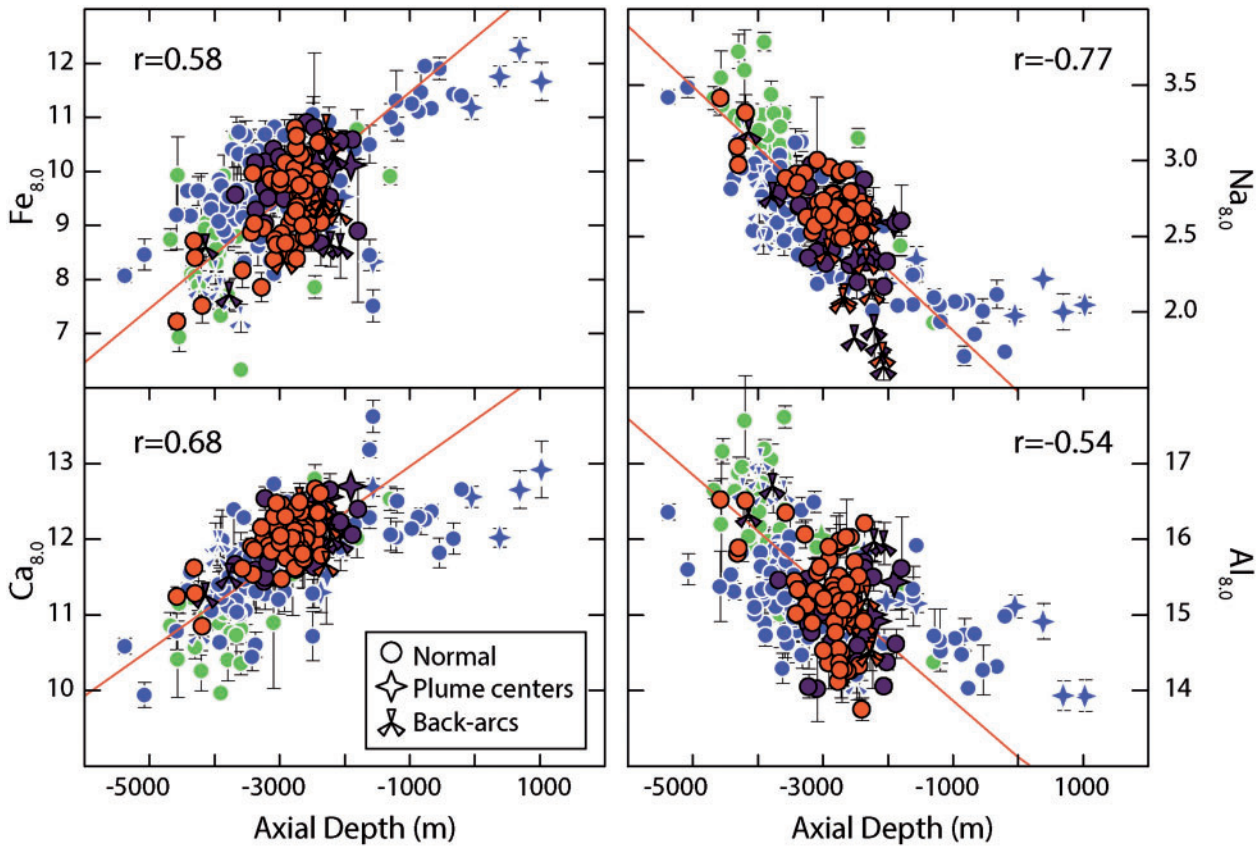

Fig. 6. $Fe_{8\cdot0}$, $Ca_{8\cdot0}$, $Na_{8\cdot0}$ and $Al_{8\cdot0}$ vs axial depth. Color tones indicate spreading rate, as in Fig. 5. Error bars are calculated as two standard deviations of the mean. Fe and Ca correlate positively with axial depth, whereas Al and Na correlate negatively. The kink in the $Na_{8\cdot0}$–depth trend associated with plume segments on and near Iceland, which are offset to higher $Na_{8\cdot0}$, should be noted. These segments also have low $Ca_{8\cdot0}$. Back-arc basin basalts (BAB) have low $Fe_{8\cdot0}$ and high $Al_{8\cdot0}$.

were not included in the early studies [e.g. Gakkel Ridge, most of the Southwest Indian Ridge (SWIR), the Pacific–Antarctic Ridge (PAR), most of the Southeast Indian Ridge (SEIR)]. The new approach to fractionation correction and inter-laboratory corrections, and the vast improvements in our knowledge of ridge depth could also change the earlier values. The previous studies and the present work, however, overlap almost exactly in $Na_{8\cdot0}$ vs ridge depth (Fig. 8). A difference in the current treatment is the inclusion of subaerial Iceland data, which do not extend the original correlation, but instead form a kink towards higher $Na_{8\cdot0}$ contents. This same kink was noted previously by Shorttle and Maclennan (2011) (see their fig. 2). The present study does extend the global range to higher $Na_{8\cdot0}$, seen in four segments from the SWIR, and to lower $Na_{8\cdot0}$, seen in five BAB segments from the Lau Basin.

The relationship between $Fe_{8\cdot0}$ and depth is also similar between the present and older studies, albeit with some noteworthy differences (Fig. 8). First among them is the large increase in the number of segment $Fe_{8\cdot0}$ values of ~8·5 at a depth of 3000 m, largely from the SEIR. In the earlier studies, data with these characteristics were highlighted as possibly a low-$Fe_{8\cdot0}$ zone related to BAB, but these results show that many normal ridge segments also possess the 'low' $Fe_{8\cdot0}$ relative to axial depth. Another difference lies in the data for the Cayman Trough. Klein & Langmuir (1987) estimated $Fe_{8\cdot0}$ values of ~7·15 for Cayman, whereas the present estimates suggest a higher $Fe_{8\cdot0}$ of between 8 and 8·5 for the Cayman segments. Other ridge segments at slightly shallower depths have low $Fe_{8\cdot0}$ contents, however, so the overall trend is little affected.

In $Ti_{8\cdot0}$ vs $Na_{8\cdot0}$, many of the same features that were pointed out by Langmuir *et al.* (1992) persist, including the lower $Ti_{8\cdot0}$ of BAB, the characteristically high $Ti_{8\cdot0}$ of Iceland segments, and the low $Ti_{8\cdot0}$ of Indian Ocean MORB for a given $Na_{8\cdot0}$. New to the present study, however, is the observation that some Gakkel segments also possess low $Ti_{8\cdot0}$ for their $Na_{8\cdot0}$, similar to the Indian Ocean signal. The results extend the lower range of observed $Ti_{8\cdot0}$ values (~0·5) with data on certain segments from the Lau Basin.

Because these data systematics are very similar in overall structure to the data summarized 20 years ago

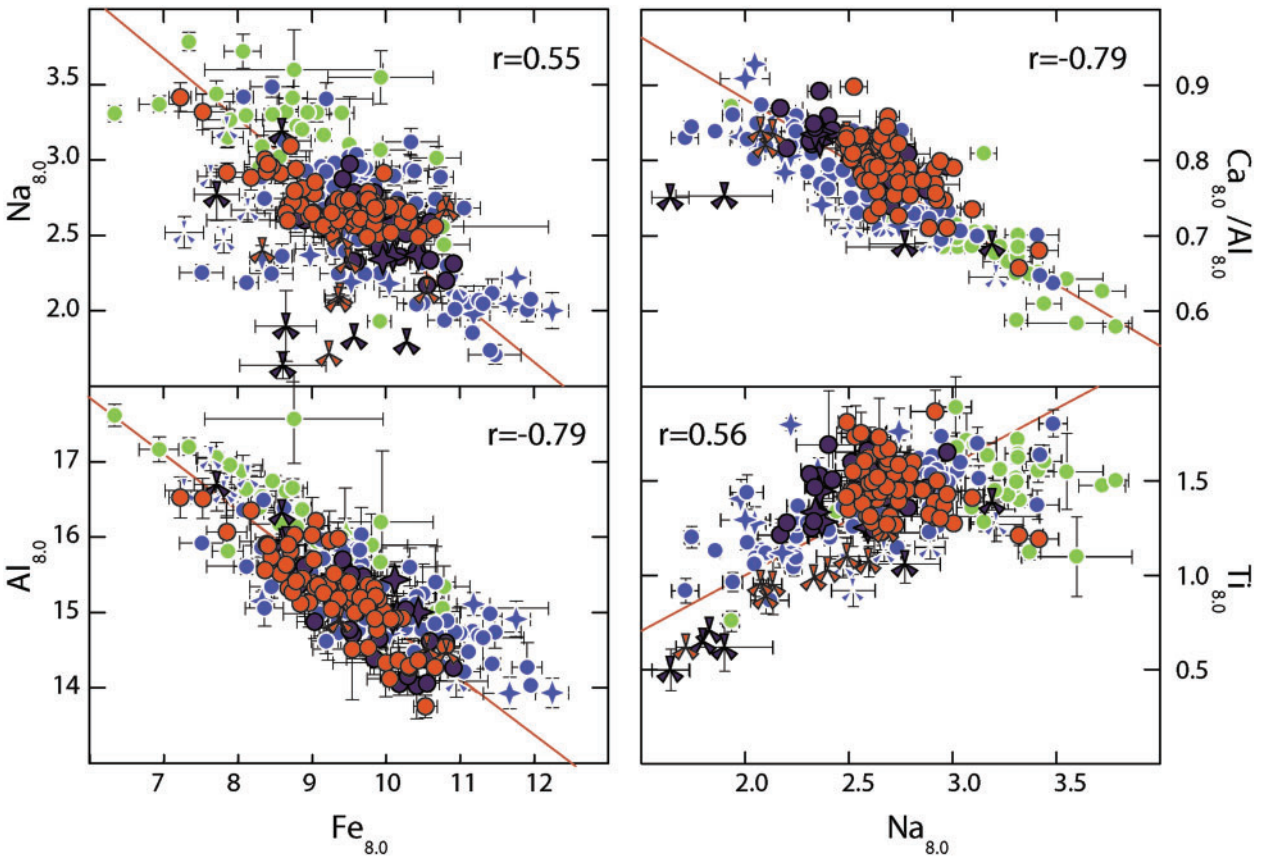

Fig. 7. $Na_{8\cdot0}$ and $Al_{8\cdot0}$ vs $Fe_{8\cdot0}$, and $Ca_{8\cdot0}/Al_{8\cdot0}$ and $Ti_{8\cdot0}$ vs $Na_{8\cdot0}$. Symbols as in previous figures. $Na_{8\cdot0}$ shows a negative correlation with $Fe_{8\cdot0}$, with the exception of BAB and a few open-ocean ridge segments near plumes. There are robust correlations between $Al_{8\cdot0}$ and $Fe_{8\cdot0}$ and $Ca_{8\cdot0}/Al_{8\cdot0}$ with $Na_{8\cdot0}$, again showing that BAB are offset to high $Al_{8\cdot0}$. Only a crude correlation exists between $Ti_{8\cdot0}$ and $Na_{8\cdot0}$. BAB are offset to low $Ti_{8\cdot0}$, forming a nearly subparallel array beneath the open-ocean ridge basalts. Superslow-spreading segments (circles) have high $Na_{8\cdot0}$ and $Al_{8\cdot0}$ relative to $Fe_{8\cdot0}$, and high $Na_{8\cdot0}$ relative to $Ti_{8\cdot0}$.

(Langmuir *et al.*, 1992), the interpretation and quantitative modeling of the data by Langmuir *et al.* (1992) in terms of mantle temperature still stands as a viable hypothesis. Critical questions that have emerged since then provide alternative hypotheses. One question is whether values corrected to 8 wt % MgO provide a suitable framework for the evaluation of mantle melting processes and mantle temperature. Niu & O'Hara (2008), for example, suggested that the values at 8 wt % MgO are largely the result of fractionation effects, and the systematics for compositions in equilibrium with mantle olivine are different, particularly for FeO. In this case, mantle temperature variations would be limited. To address this question adequately requires correction of the data back to equilibrium with mantle olivine, so that the different correction procedures can be compared. A second question is whether variations in mantle composition might account for the observations (e.g. Shen & Forsyth, 1995; Niu & O'Hara, 2008). A third is whether melt transfer processes ('melt–rock reaction') might be able to produce the same correlations among the 8-parameters through interaction with the lithosphere during magma ascent (e.g. Kimura & Sano, 2012). We address all of these questions below.

Calculating liquids in equilibrium with Fo_{90} mantle olivine

To determine the possible interpretative consequences of correction to 8 wt % MgO or equilibrium with Fo_{90} olivine, compositions in equilibrium with Fo_{90} were also calculated for every sample with an 8-value in the database. This is equivalent to a correction to constant Mg# [atomic Mg/(Mg + Fe)], advocated, for example, by Niu & O'Hara (2008). Such corrections move the normalized values outside the range of MORB data, and are critically dependent on the choice of the MgO content (hence Mg#) of plagioclase appearance. In MORB, plagioclase generally appears at near-constant MgO, but very different Mg#, which means corrections need to be done with explicit assumptions and great care.

In this study, the 90-values are determined for most samples with plagioclase joining olivine at 8·5 wt % MgO, consistent with LLD calculations for many

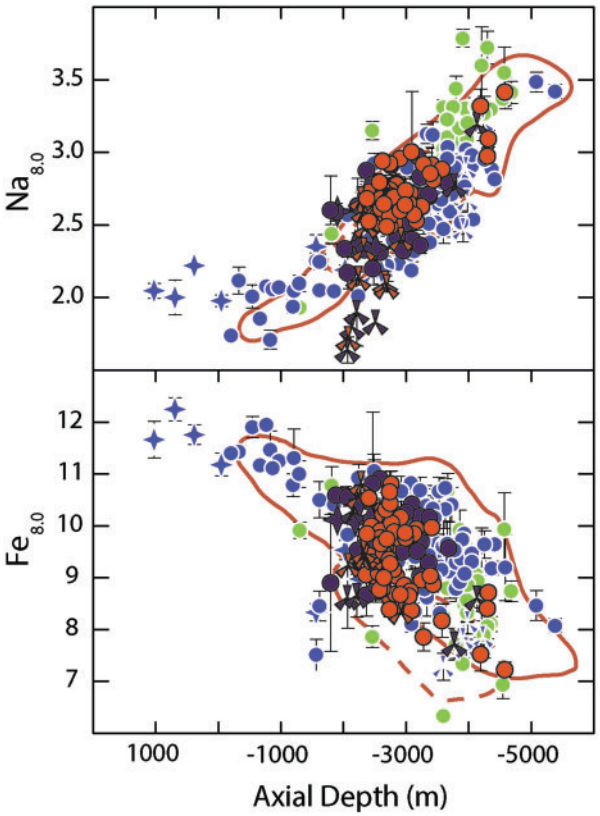

Fig. 8. $Na_{8·0}$ and $Fe_{8·0}$ vs axial depth from this study (symbols as in previous figures) compared with that of Langmuir *et al.* (1992) (outlined fields: continuous line, open-ocean ridge field; dashed line, BAB field). The good correspondence between the data from this study and from that of Langmuir *et al.* (1992) should be noted. The present study extends the range in axial depth by including subaerial Iceland segments. The range in $Na_{8·0}$ is also expanded through the inclusion of data from the Gakkel Ridge and the SWIR (high $Na_{8·0}$) and certain Lau back-arc segments (low $Na_{8·0}$) that were unavailable in previous compilations. In $Fe_{8·0}$, there are more segments with a value of ~8·5 at 3500 m depth, extending into a region previously outlined by Langmuir *et al.* (1992) as the BAB zone. Even with a vast increase in data, and the improved fractionation correction procedure carried out here, the original Langmuir *et al.* (1992) correlations remain robust.

MORB, and also with the method used by Langmuir *et al.* (1992) to crystallize their mantle melt compositions to 8 wt % MgO to compare with MORB compositions. The choice of when plagioclase begins to crystallize is critical for the calculation of the Fo_{90} normalized values. Kinzler (1997) and Till *et al.* (2012), for example, used a much higher MgO of plagioclase first appearance. As noted by Till *et al.* (2012), this has a significant effect on the calculated temperatures and pressures of generation of MORB primary magmas. Because the slope on a plot of MgO–FeO is approximately 1·4–1·6, changing the 'plagioclase-in' from 8·5 to 10·5 wt % MgO can lower the inferred FeO of primary melts (those in equilibrium with the mantle) by 2·8–3·2%, much of the total range. The overall lower FeO would also make calculated mantle temperatures and pressures much lower.

Indeed, for the evaluation of the various hypotheses, the range of FeO in MORB primary magmas is critical. The new observations presented above show there is generally a negative correlation observed between Al_2O_3 and FeO contents in MORB (Fig. 7), so the range in FeO is closely tied to the variation in Al_2O_3. Is this correlation produced by melting or crystallization? The correlation is consistent with different extents of melting, because higher temperatures lead to a greater depth of melting, creating higher FeO melts (Hanson & Langmuir, 1978; Klein & Langmuir, 1987), and also produce a larger melt fraction, lowering Al_2O_3, as Al behaves moderately incompatibly during melting. Melting of colder mantle begins shallower and produces compositions with lower FeO contents and less melting overall, leading to higher Al_2O_3 contents. Hence variable mantle temperature produces an inverse correlation between the two parameters. Such behavior is also evident in MELTS calculations (e.g. Asimow *et al.*, 2001). A negative correlation between $Al_{8·0}$ and $Fe_{8·0}$ could also be produced, however, by varying the MgO of plagioclase appearance—plagioclase removal causes Al_2O_3 to decrease and FeO to increase. Early plagioclase appearance would lead to high-FeO, low-Al_2O_3 magmas, and late appearance to low-FeO, high-Al_2O_3 magmas.

If plagioclase appears at variable MgO contents, and primary magmas with the same FeO had different MgO of plagioclase appearance during crystallization, then a large range in $Fe_{8·0}$ could be generated despite primary magmas with no difference in FeO content. High $Fe_{8·0}$ would relate to a high MgO of plagioclase appearance, and low $Fe_{8·0}$ to a low MgO of plagioclase appearance. So which factor is the primary cause of the observed Al–Fe relationship? Could a variable 'plagioclase-in' cause the various correlations seen at 8 wt % MgO?

To evaluate this question requires an understanding of (1) the MgO content at which plagioclase appears on the liquidus, and (2) how this may vary across the range of MORB compositions. These questions can be addressed both from an understanding of phase equilibria and from considering the MORB glass data. We turn first to consideration of phase equilibria.

As shown by Roeder & Emslie (1970), Hanson & Langmuir (1978), Langmuir & Hanson (1980) and Weaver & Langmuir (1990), the stability of olivine depends on the total amount of MgO and FeO in the liquid according to the equation

$$K_d^{MgO} \times MgO_{Liq} + K_d^{FeO} \times FeO_{Liq} = 66 \cdot 67 \quad (1)$$

where K_ds are partition coefficients that decrease with increasing temperature and also have some compositional dependence [e.g. see Langmuir *et al.* (1992), among others]. From this equation it is clear that at a constant

MgO content of the liquid, increased FeO increases the stability of olivine. For plagioclase, the analogous stability equation is

$$K_d^{An} \times An_{Liq} + K_d^{Ab} \times Ab_{Liq} = 1{\cdot}0. \quad (2)$$

It is important to note that it is the anorthite content, not the calcium content, nor the Ca/(Ca + Na) ratio, that is essential, because Ca can be in both plagioclase and clinopyroxene components. Normative anorthite in a cation norm is (Al − Na)/0·4, and is largely dependent on the Al_2O_3 content of the melt. [Increasing clinopyroxene components in the liquid, which increases CaO, does not increase the stability (i.e. temperature of first appearance) of plagioclase. This is illustrated, for example, in the plagioclase–diopside ternary phase diagram common in petrology.] These considerations then assist an evaluation of the relative stabilities of olivine and plagioclase in MORB compositions.

From examination of equations (1) and (2), high-FeO, low-Al_2O_3 melts would stabilize olivine and destabilize plagioclase, leading to plagioclase crystallization at lower Mg#, whereas the low-FeO, high-Al_2O_3 melts will crystallize plagioclase at higher Mg#. Therefore Reykjanes Ridge MORB compositions, with high FeO and low Al_2O_3, should have plagioclase stability at lower MgO or Mg# than Gakkel Ridge and SWIR basalts, which have very low FeO and high Al_2O_3. These points are illustrated in Fig. 9, which shows in particular the very large range of Mg# over which plagioclase-in occurs. In contrast, there is a limited range of MgO for plagioclase appearance, because high-FeO magmas have a much lower Mg# for a given MgO content. These considerations are consistent with the reasoning of Winpenny & Maclennan (2011), who also pointed out the lower Mg# of phase appearance for higher-pressure magmas.

But there could be some other effect that is changing plagioclase appearance that we are not considering, such as variable volatile content, the effects of pressure and so on. If we were to force variable plagioclase-in to account for the $Fe_{8\cdot0}$–$Al_{8\cdot0}$ correlation, would that produce the necessary changes in the other elements? This is explored in Fig. 10, which demonstrates how varying the MgO content of plagioclase appearance by 3 wt % could in fact lead to the $Fe_{8\cdot0}$–$Al_{8\cdot0}$ correlation, but then would produce a positive correlation between $Fe_{8\cdot0}$ and $Na_{8\cdot0}$ and a negative correlation between $Na_{8\cdot0}$ and $Al_{8\cdot0}$—the opposite of the observations. There is, however, substantial spread in the correlations of the natural data, to which variable plagioclase-in could contribute, as discussed further below.

The MgO content of plagioclase appearance can also be revealed by MORB data, because plagioclase appearance causes FeO and TiO_2 to increase rapidly with MgO, and Al_2O_3 to decline with a slope of ~1 on a plot of MgO–Al_2O_3. There is an additional test from trace elements. Sr has a partition coefficient of about two in plagioclase. During mantle melting, plagioclase does not play an important role, and Sr and Nd have similar partition coefficients, so the Sr/Nd ratio of mantle melts reflects the source value. Once plagioclase begins to crystallize, the partition coefficient for Nd remains low, but that for Sr greatly increases, causing the Sr/Nd ratio to decrease rapidly. Estimated mantle values for Sr/Nd range from 13·7 for the depleted mantle (Salters & Stracke, 2004) to 15·9 for the primitive mantle (Sun & McDonough, 1989). Magmas with these values are unlikely to have undergone substantial plagioclase removal, unless the mantle source had much higher values of Sr/Nd. These various effects of plagioclase removal can be evaluated using data from MORB glasses, which should then indicate where plagioclase appears.

Data from two segments on the MAR are shown in Fig. 11, chosen to reflect much of the global range in axial depth. The shallow Reykjanes Ridge (RR) segment has higher $Fe_{8\cdot0}$ and lower $Al_{8\cdot0}$, evident from the figure, and also lower Sr and TiO_2 contents compared with the Kane segment. For these compositions to be related to a parent with the same FeO content, the RR parent would have to crystallize plagioclase starting at very high MgO, of 11 wt % or more, and the Kane parent at much lower MgO. If this occurred, however, then the discrepancy in TiO_2 content would be even greater. For the TiO_2 content of the parental magmas to be similar, the Kane parent would have to crystallize plagioclase at much higher MgO and the RR parent at lower MgO. In either of these scenarios, the Sr/Nd ratio should show marked changes at >8 wt % MgO, and should not reach mantle source values until 11 wt % MgO. Instead, mantle source values are reached near 8·5 wt % MgO. From this reasoning it is apparent there is no solution whereby changing plagioclase appearance can yield a common parental magma. In addition, calculated LLD for high-MgO lavas from the two regions pass directly through the data, with plagioclase appearing between 8 and 8·5 wt % MgO, just where the Sr/Nd ratio reaches mantle values.

Data, petrological reasoning, calculations and trace element constraints all demonstrate, therefore, that a variable MgO of plagioclase appearance is not a reasonable explanation for the large variations in $Fe_{8\cdot0}$ that are present in the data. Instead, if anything, the high $Fe_{8\cdot0}$ magmas crystallized plagioclase at slightly lower rather than higher MgO (see Fig. 11). In general, the end-members of MORB compositions crystallize plagioclase over a limited range of MgO (with the exception of hydrous compositions, discussed further below), and a wide range of Mg#.

Although variable plagioclase-in cannot produce the principal component of variation of the data, it is apparent from Figs 7 and 10 that the $Fe_{8\cdot0}$–$Al_{8\cdot0}$ correlation is much

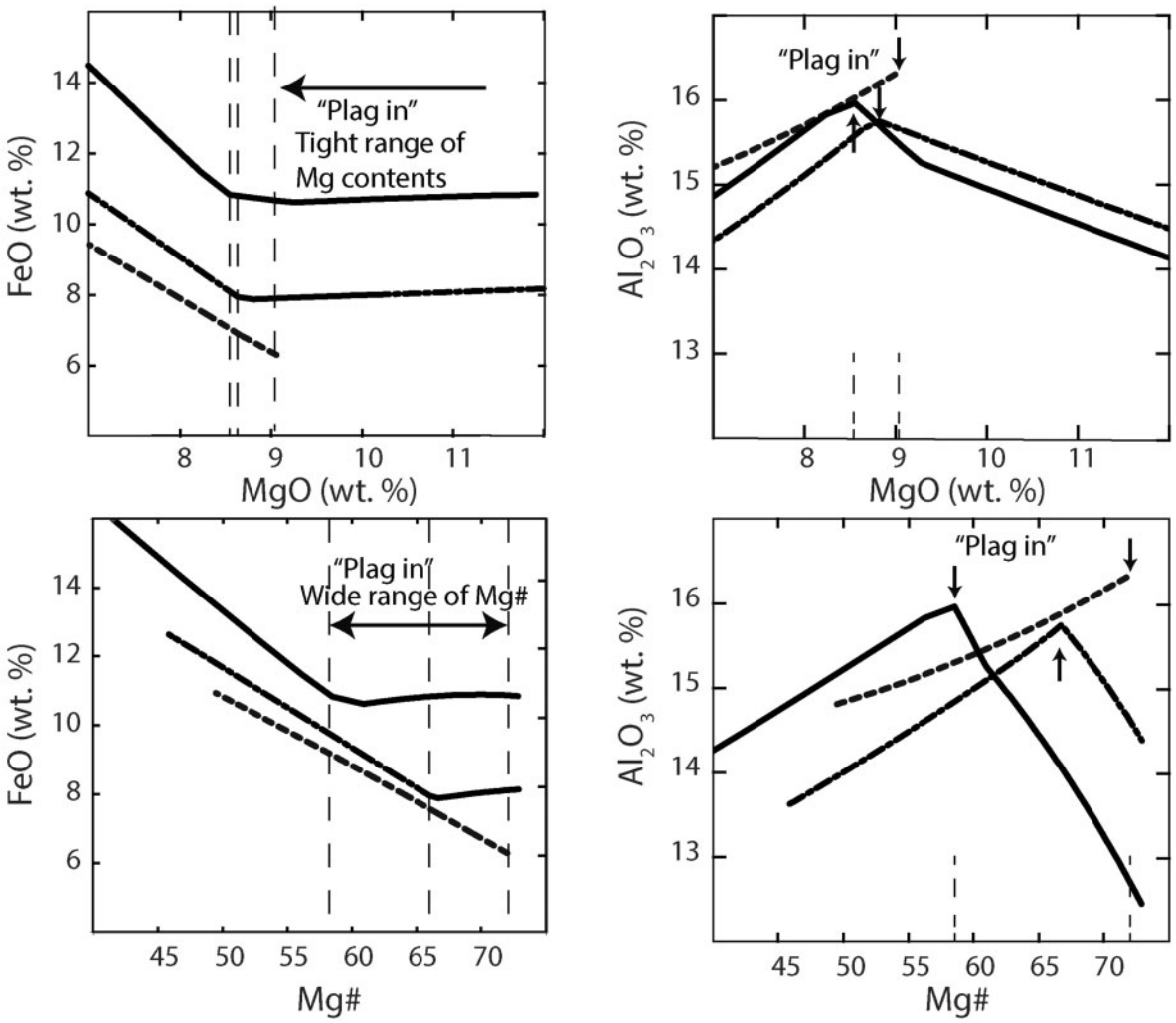

	SiO_2	TiO_2	Al_2O_3	FeO	MgO	CaO	Na_2O	K_2O
Low-Fe parental melt	50.81	1.03	16.34	6.25	9.05	13.42	2.76	0.24
Med-Fe parental melt	50.31	0.84	14.39	8.1	12.25	11.67	2.24	0.11
High-Fe parental melt	46.81	0.99	12.45	10.82	16.33	11.02	1.39	0.09

Fig. 9. Diagrams showing LLD (variably dashed lines calculated using hBasalt; Bezos *et al.*, in preparation) from high-FeO, medium-FeO and low-FeO parental magmas. It should be noted that all three magmas begin crystallizing plagioclase (indicated by dashed vertical line) at a narrow MgO interval near 8·5 wt %. In contrast, the three magmas begin crystallizing plagioclase at a wide range of Mg# [atomic Mg/(Mg + Fe)]. High-FeO (low-Al_2O_3) magmas crystallize plagioclase at much lower Mg# than low-FeO (high-Al_2O_3) magmas. This demonstrates the benefit of fractionation correction based on MgO, which is applicable to a wide compositional range, as opposed to the Mg# approach. Compositions of the parental magmas are given in the table at the bottom of the figure.

tighter than the $Na_{8\cdot0}$–$Al_{8\cdot0}$ or $Na_{8\cdot0}$–$Fe_{8\cdot0}$ correlations, for which the correlation coefficient drops from 0·79 to 0·55. This may be a consequence of a variable MgO content of plagioclase appearance. As shown in Fig. 10, variable plagioclase-in produces corrected values similar to the observed $Fe_{8\cdot0}$–$Al_{8\cdot0}$ trend, but orthogonal to the $Na_{8\cdot0}$–$Al_{8\cdot0}$ or $Na_{8\cdot0}$–$Fe_{8\cdot0}$ trends. We conclude that the principal component of data variation cannot result from variations in fractionation path from primitive mantle melts, but that the spread of the data on $Na_{8\cdot0}$–$Al_{8\cdot0}$ and $Na_{8\cdot0}$–$Fe_{8\cdot0}$ probably relates at least in part to variable plagioclase-in.

In view of this analysis, we adopt a plagioclase appearance at 8·5% MgO as approximately correct for the universe of MORB compositions, and also recognize the need to consider in the data the likelihood that plagioclase appearance may vary from ~7·5% to 9·5% MgO in

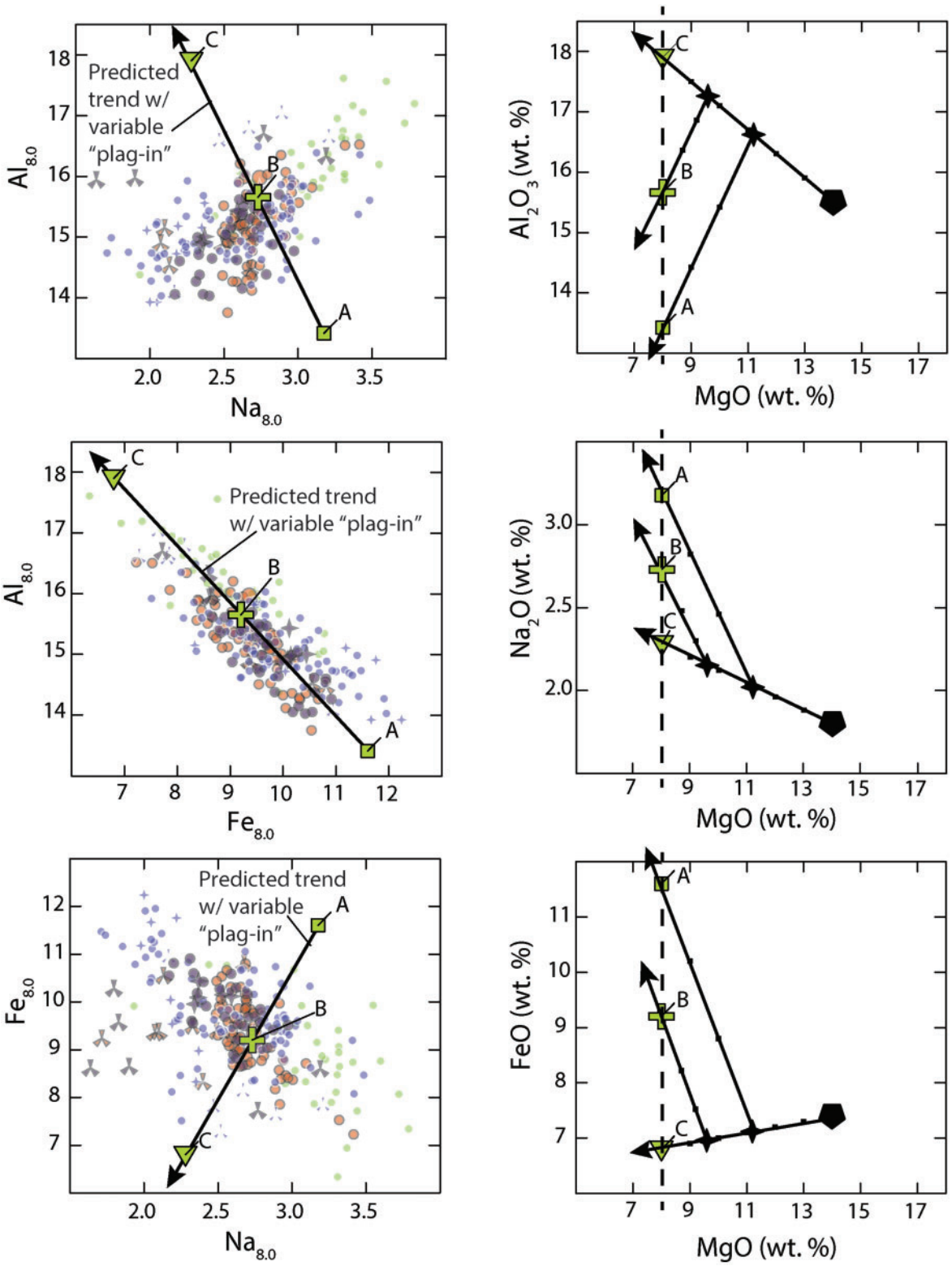

Fig. 10. Al_2O_3, Na_2O and FeO vs MgO; $Al_{8\cdot0}$ vs $Na_{8\cdot0}$ and $Fe_{8\cdot0}$, and $Fe_{8\cdot0}$ vs $Na_{8\cdot0}$. Shown is a single parental magma (black pentagon), with three different 'plagioclase-in' values (sample LLDs shown as black lines; the three different magmas created by variable plag-in are labeled A, B, C to aid comparison). It should be noted that the observed global range in $Al_{8\cdot0}$, $Na_{8\cdot0}$ and $Fe_{8\cdot0}$ can be achieved simply though varying the MgO of plagioclase-in, but the relationships between oxides are inconsistent with the global array. For example, the correlation between $Al_{8\cdot0}$ and $Na_{8\cdot0}$ predicted owing to variable plag-in is negative, whereas the global MORB data show a positive relationship between $Al_{8\cdot0}$ and $Na_{8\cdot0}$. That variable plag-in can lead to an effect orthogonal to the $Fe_{8\cdot0}$–$Na_{8\cdot0}$ and $Al_{8\cdot0}$–$Na_{8\cdot0}$ arrays, but one parallel to the $Fe_{8\cdot0}$–$Al_{8\cdot0}$ array, might explain the increased 'noise' in the $Fe_{8\cdot0}$–$Na_{8\cdot0}$ and $Al_{8\cdot0}$–$Na_{8\cdot0}$ trends.

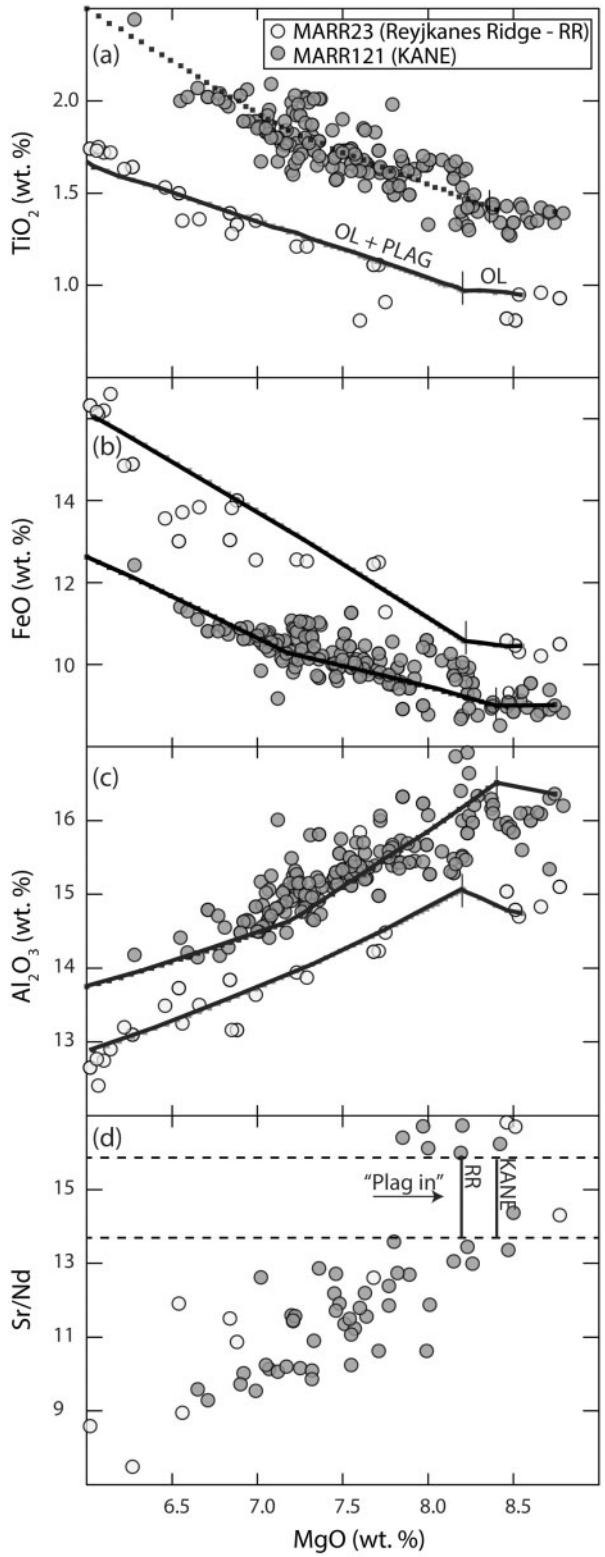

Fig. 11. TiO_2, FeO, Al_2O_3 and Sr/Nd vs MgO for MARR23 (RR, Reykjanes Ridge), which has a depth of 800 m, and MARR121 (Kane segment), which has a depth of 4000 m. It should be noted that RR has higher $Fe_{8\cdot0}$ and lower $Ti_{8\cdot0}$ than Kane. Data from both segments correspond to calculated LLD (Petrolog; Danyushevsky & Plechov, 2011) where olivine crystallizes alone to less than 9 wt % MgO, joined by plagioclase at 8·5 wt % MgO for Kane and 8·1 wt % for RR. Thus plagioclase appears at about the same MgO content across the broad range of MORB compositions. If instead Kane and RR were derived from the same parental magma with different crystallization histories, much earlier plagioclase crystallization would be required to drive up the FeO contents of the RR magmas. Such early entry of plagioclase is inconsistent with the low TiO_2 contents of RR. Another test of plagioclase appearance is the Sr/Nd ratio (d), as Sr is a compatible element in plagioclase and decreases once plagioclase appears on the liquidus, but behaves similarly to Nd during mantle melting and olivine crystallization. After plagioclase appears on the LLD, Sr/Nd drops rapidly relative to mantle values, which are indicated by dashed lines in (d). Above 8 wt % MgO, magmas from both segments have Sr/Nd similar to the range of primitive mantle at 15·9 (Sun & McDonough, 1989) to depleted mantle at 13·7 (Salters & Stracke, 2004). Thus major element data, trace element data and calculated LLD are all consistent with plagioclase appearance between 8 and 8·5% MgO. Much higher values of MgO for plagioclase appearance are not justified by MORB data.

certain cases. In practice, to generate Fo_{90} compositions, every sample (with <8·5 wt % MgO) was first corrected to its value at 8·5 wt % MgO following the method outlined in the Supplementary Data for 8-values, because 8·5 wt % MgO is the normal 'hinge-point' where the slope changes to olivine-only. Olivine was then added in 0·1% increments to these compositions until they were in equilibrium with Fo_{90}. Samples with greater than 8·5 wt % MgO are already on the olivine-only slope and so required no correction apart from olivine addition to be in equilibrium with Fo_{90}. For olivine addition, a K_D $(C_{ol}^{FeO}/C_L^{FeO})/(C_{ol}^{MgO}/C_L^{MgO}) = 0{\cdot}3$ was used. Once all sample compositions had been corrected to equilibrium with Fo_{90} olivine, those samples were averaged to estimate a segment 90-value for each segment with 8-values.

For back-arc basins, the plagioclase-in value was modified for certain high-H_2O segments to 7·5 wt % MgO (see Supplementary Data for details) when calculating segment 8- and 90-values. In general, accounting for water when correcting for fractionation is imperfect, as water is measured in so few samples. As such, the approach taken here was to change the plagioclase-in value only for certain BAB segments or where the variation diagrams showed compelling evidence of a lower value (e.g. SWIR4). Although there may be enriched (E)-MORB segments that are higher-H_2O than typical MORB, that level of detailed adjustment went beyond the scope of this study.

Comparison of corrections to constant MgO vs constant Mg/Fe

An important issue to address is whether correction to a constant MgO content or constant Mg/Fe ratio makes a difference to the data systematics. Figure 12 compares 8-values and 90-values for the global ridge segments. There are very tight correlations between the two sets of

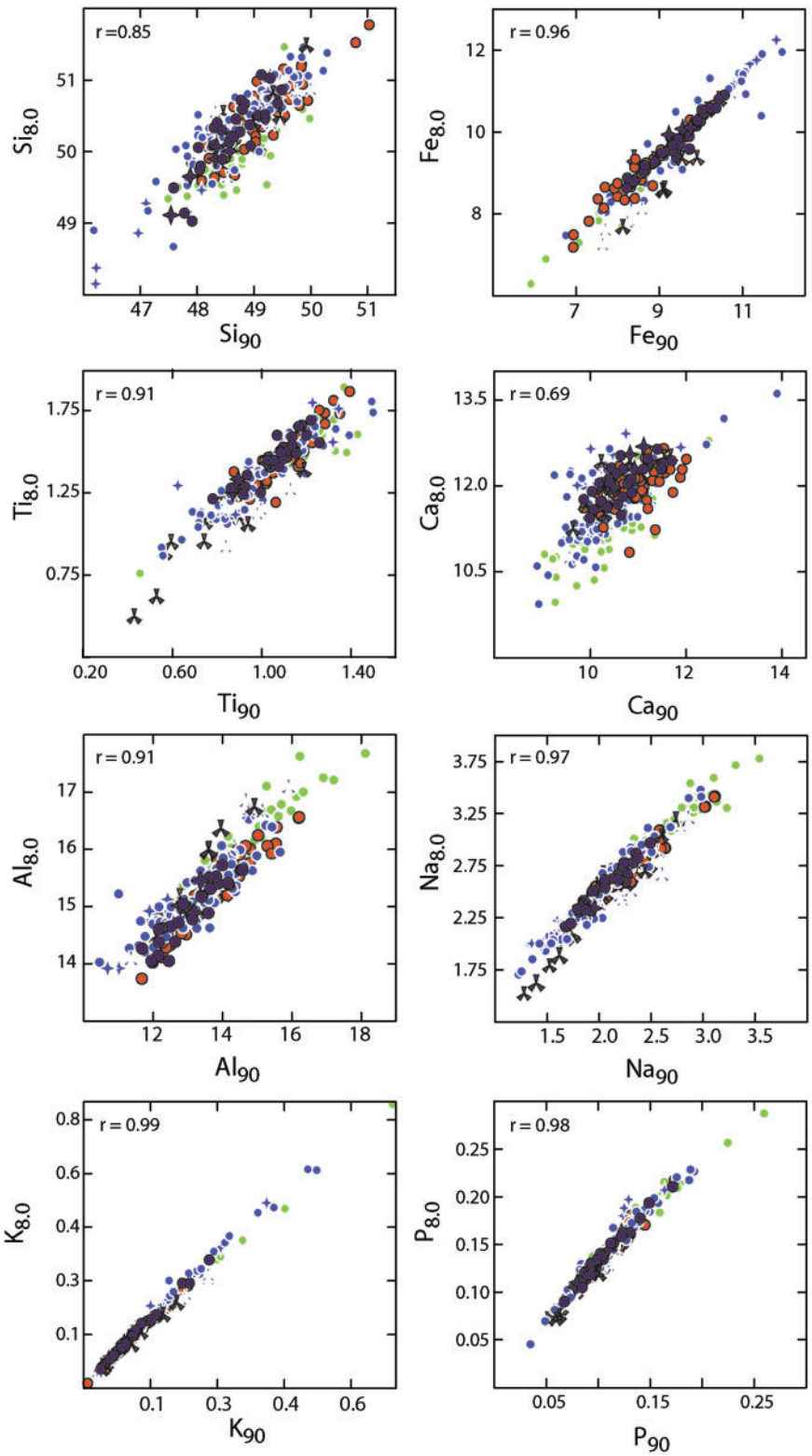

Fig. 12. Segment 8-values vs segment 90-values for the major oxides SiO_2, TiO_2, Al_2O_3, FeO, CaO, Na_2O, K_2O and P_2O_5. Symbols as in previous figures. It should be noted that there are very tight correlations between the two sets of corrected values for most elements. The correlations are not 1:1, however. The elements TiO_2, Al_2O_3, Na_2O and SiO_2 have a larger range in 90-values than they do in 8-values, related to their negative correlations with $Fe_{8\cdot0}$. Samples with high $Fe_{8\cdot0}$ tend to have low $Al_{8\cdot0}$, $Na_{8\cdot0}$, $Ti_{8\cdot0}$ and $Si_{8\cdot0}$ and also require the greatest amount of olivine addition to be in equilibrium with Fo_{90} olivine. Therefore, the already low Al, Na, Ti and Si-$_{8\cdot0}$ samples become even lower during correction to Fo_{90}. Ca is more complicated, as it correlates positively with $Fe_{8\cdot0}$. Therefore high $Ca_{8\cdot0}$ samples are lowered more during correction, and low $Ca_{8\cdot0}$ samples are lowered less during correction, precluding a tight correlation between $Ca_{8\cdot0}$ and Ca_{90}.

corrected values for most elements. The offsets between 8- and 90-values depend on the Mg/Fe at 8 wt % MgO. Samples with high $Fe_{8\cdot0}$ values, and hence low Mg/Fe at 8 wt % MgO, have large corrections to arrive at equilibrium with Fo_{90}, whereas samples with low $Fe_{8\cdot0}$ values have negligible corrections. The effect of the correction also varies for the different elements. Adding olivine to arrive at a composition in equilibrium with Fo_{90} does not change FeO much, but increases MgO. Elements that are not incorporated in olivine (Al_2O_3, Na_2O, TiO_2 and CaO) are decreased by dilution. SiO_2 is also lowered because olivine has lower SiO_2 than MORB. Because segments with high $Fe_{8\cdot0}$ have the lowest $Al_{8\cdot0}$, $Na_{8\cdot0}$, $Ti_{8\cdot0}$, and $Si_{8\cdot0}$, the extensive olivine addition creates even lower 90-values, amplifying the variation in these elements. In contrast, high-$Fe_{8\cdot0}$ magmas have high $Ca_{8\cdot0}$, so correction to Fo_{90} reduces the range of variation of Ca_{90} relative to $Ca_{8\cdot0}$.

These factors then lead to an expansion of the range of Al_{90}, Na_{90}, Si_{90} and Ti_{90} relative to $Al_{8\cdot0}$, $Na_{8\cdot0}$, $Si_{8\cdot0}$ and $Ti_{8\cdot0}$, and excellent correlations for these elements between 8-values and 90-values. The contrasting behavior of Ca leads to a less good correlation between $Ca_{8\cdot0}$ and Ca_{90}. The important aspect, of course, is the comparison of the data with models of mantle melting and mantle composition, and not the existence of a correlation or not, as discussed below.

The net result is that the data systematics for 8-values and 90-values are remarkably similar. The same correlations exist with depth, with the exception of Ca_{90}. The inter-element correlations are generally tighter in the 90-values, in part because of the mutual 'stretching' of the data discussed above. Fe_{90}–Al_{90}–Na_{90} correlations are particularly pronounced, and there is also a good Si_{90}–Fe_{90} correlation and a much better Ti_{90}–Na_{90} correlation (Fig. 13). Whatever the explanation for these striking systematics, they are not an artifact of the correction method. The same systematics exist whether data are corrected to 8 wt % MgO or equilibrium with Fo_{90}.

Are 8-values or Fo_{90} values preferable?

There is a question of whether correction to 8 wt % MgO or Fo_{90} has an important effect on inferences for mantle processes. Indeed, a criticism of the 8-value approach has been that the resulting compositions are not in equilibrium with mantle olivine (Niu & O'Hara, 2008). This criticism reflects a misunderstanding, as Klein & Langmuir (1987) and Langmuir *et al.* (1992) never claimed that 8-values were in equilibrium with mantle olivine; rather, they selected 8 wt % MgO because it is in the field of observed basalt compositions. Thus nearly all mean segment 8-values are pinned to data near 8 wt % MgO that require little or no correction. To directly compare 8-values with mantle melting models, Langmuir *et al.* (1992) and Kinzler (1997) calculated mantle melts and fractionated them to 8 wt % MgO. Taking mantle melts and fractionating them to 8 wt % MgO, or taking 8 wt % MgO values and back-correcting them to equilibrium with Fo_{90} leads to identical results provided the LLD are consistent. Carrying out forward calculations from mantle melts and comparing with 8-values has the advantage that the LLD of the mantle melts are constrained and phase appearances are determined by the calculated LLD. As discussed at length above, back-calculating to Fo_{90} is less constrained, because the choice of phase disappearance can be arbitrary. This principle can be understood from considering a ternary phase diagram. Any LLD can be uniquely determined from a given starting composition. However, a given liquid that lies on a cotectic can come from an infinite variety of higher temperature parental compositions, and the choice of where it leaves the cotectic to pass into a single-phase field cannot be known. Backtracking cannot be performed accurately without independent constraints.

Because LLD can in principle be calculated accurately for experimental melt compositions, there is less uncertainty in comparing 8-values with fractionated mantle melts. But it is also convenient to be able to compare 90-values directly with the experiments. In either case, provided the corrections to the basalt data can be applied correctly (see above), the results should be the same. With careful data treatment, therefore, 8-values and Fo_{90} values lead to identical results.

Fine structure within the global correlations

Important additions in the present study, in addition to the thorough data treatment and documentation, are the inclusion of $Al_{8\cdot0}$, $Ca_{8\cdot0}$, $Si_{8\cdot0}$ and $P_{8\cdot0}$ for all of the ridge segments, the consideration of corrections both to 8 wt % MgO and equilibrium with Fo_{90} olivine, a quantitative and reproducible approach to segment depth, the quantification of errors, and the inclusion of spreading rate for each segment, which permits exploration of variations with spreading rate. These improvements reveal relationships that were not known previously.

As noted above there is much more variation within the data than can be accounted for by a single uniform process. A full exploration of the detailed structure of the data would require work on a finer scale than segment averages that would concentrate on highly sampled regions. Here we point out only some of the notable aspects of the data.

Superslow-spreading ridges

Superslow-spreading ridges are represented by the SWIR and the Gakkel Ridge, both spreading at <15 mm a^{-1}, as well as two segments from the Red Sea. Segments from Gakkel and the SWIR are preponderant at the greatest depths and highest Na_2O contents of the global dataset, although SWIR segments can also be as shallow as 2400 m. Fortunately, the Australian–Antarctic Discordance, which

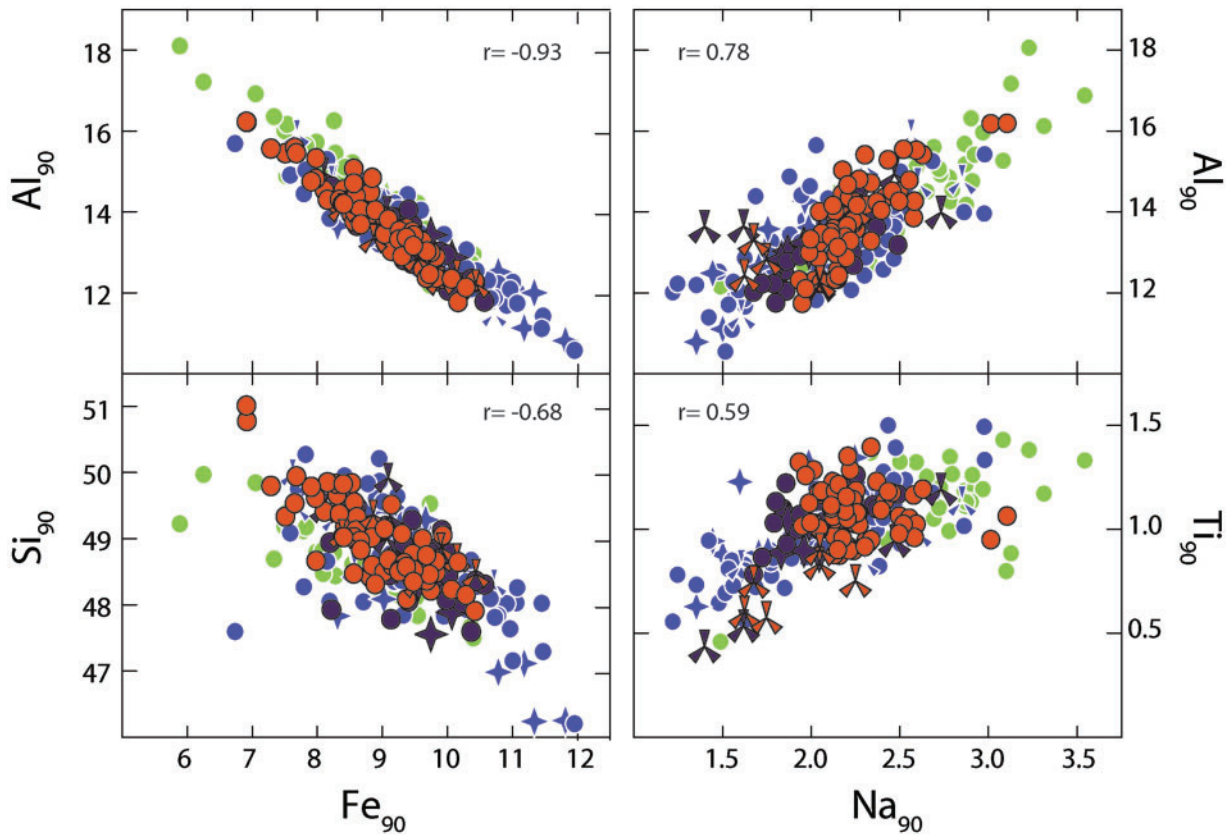

Fig. 13. Al_{90} and Si_{90} vs Fe_{90}, and Al_{90} and Ti_{90} vs Na_{90}. Symbols as in previous figures. The strong correlations, especially in Al_{90} vs Fe_{90}, should be noted. Most of the correlations observed among the segment 8-values persist in the 90-values, in many cases becoming even more pronounced.

is intermediate spreading, occupies the same depth range; it is therefore possible to separate variables and identify which aspects of the data are unique to the superslow-spreading ridges.

When plotted versus Fe_{90}, the superslow-spreading ridges are offset to lower Si_{90} and Ca_{90}, and higher Na_{90} and Al_{90} compared with faster-spreading ridges, forming fields that only slightly overlap (Fig. 14). Although there are a few exceptional segments, these offsets seem to exist across the entire depth range. Clearly there is some additional effect, presumably associated with lithospheric cooling, that causes these offsets relative to other ridges and needs to be explained, as discussed further below.

Ridges near hotspots

A second effect has to do with segments that are located in the vicinity of hotspots. There are multiple features to these effects, and they are not necessarily uniform from one hotspot to another. One effect is that at hotspot centers there is an elevation of Na_2O relative to what would be expected from the $Na_{8\cdot0}$–depth correlation observed elsewhere (see the kink in the $Na_{8\cdot0}$–depth trend in Iceland segments in Fig. 6). This can be illustrated by calculating the $Na_{8\cdot0}$ anomaly relative to the $Na_{8\cdot0}$–depth relationship of open-ocean segments far from hotspots. Figure 15 shows the elevated Na_2O at the centers of the Azores and Iceland hotspots relative to their adjoining segments. Importantly, the positive Na_2O anomaly over plume centers is also associated with elevated K_{90} and $^{87}Sr/^{86}Sr$ (Fig. 15), suggesting that source enrichment is responsible for the hotspot center effects.

At the same time there is a tendency for the margins of several hotspots to be exceptionally low in $Na_{8\cdot0}$ for their depth. For example, the FAMOUS segment on the Mid-Atlantic Ridge has an $Na_{8\cdot0}$ of 2·25, despite its depth of 2700 m. Segments of the East Pacific Ridge (EPR) at the same depth have $Na_{8\cdot0}$ of about 2·6. Similarly, Reykjanes Ridge segments distant from Iceland have $Na_{8\cdot0}$ of 2·0, despite being as deep as 2250 m. These relationships can lead locally to a positive correlation between $Na_{8\cdot0}$ and depth—deepest segments have the lowest $Na_{8\cdot0}$. Clearly the systematics adjacent to hotspots have additional complexities influencing their chemical compositions.

There is a question of whether there are significant variations along ridges apart from a 'hotspot effect', which would lead to the interpretation of very limited chemical and temperature variations along 'normal' ocean ridges (e.g. Shen & Forsyth, 1995). Langmuir *et al.* (1992) claimed

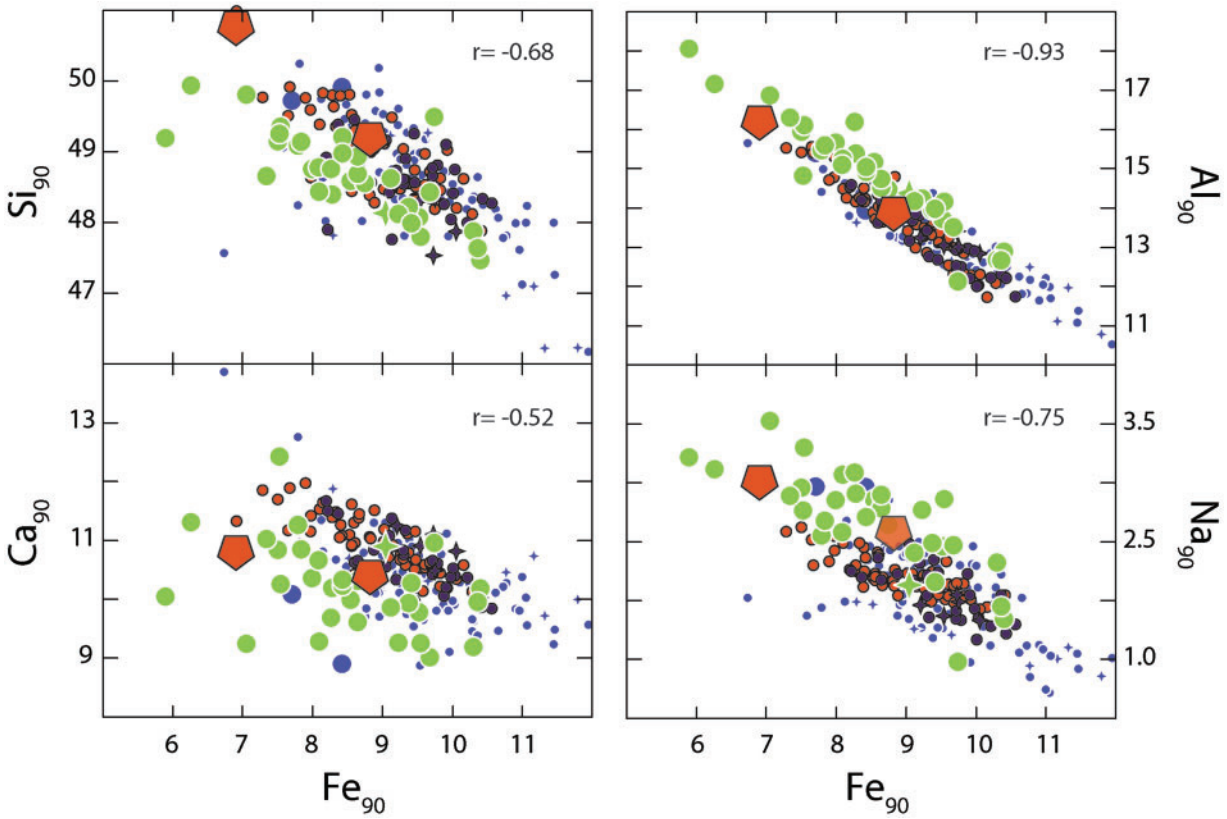

Fig. 14. Si_{90}, Ca_{90}, Al_{90} and Na_{90} vs Fe_{90}, highlighting the systematics in superslow-spreading ridge segments. Symbols as in previous figures, although symbol size from faster-spreading segments has been reduced by 50% to aid visualization. Two segments from the AAD are shown in large pentaagons as a point of comparison, as these segments are in the depth range of most superslow-spreading segments but are intermediate-spreading. Differences between the AAD and superslow-spreading segments are probably related to a spreading rate effect. The very deep segments from the Cayman Trough are also shown by dark, large circles for comparison. It should be noted that superslow-spreading segments, with few exceptions, are offset to low Si_{90} and Ca_{90}, and high Al_{90} and Na_{90} relative to faster-spreading segments. This is probably caused by the cold lithospheric cap present at superslow-spreading segments (see discussion in text).

large variations for 'normal ridges'. This apparent disagreement is in part a matter of semantics. Schilling (1975) defined 'normal' as basalts that were depleted in the light rare earth elements (LREE). Using this definition, which was that adopted by Langmuir *et al.* (1992), most segments of the Kolbeinsey Rise and Reykjanes Ridge are 'normal'. Also Iceland, with its high $Fe_{8\cdot0}$, generally plots on extensions of other ridges on most variation diagrams. The MAR near the Azores, in contrast, has low $Fe_{8\cdot0}$ despite shallow ridge depths, illustrating that some hotspots are abnormal in terms of their relationships between chemical parameters and depth. Therefore it is appropriate to make distinctions for some hotspots with anomalous chemistry. Inclusion of the LREE-depleted ridges near Iceland provides a total depth range of <1000 to 5000 m, encompassing almost the entire range of ocean ridge depths. Most importantly, as ridges are passive features, they sample the temperature of the mantle over which they pass. If that happens to be a hotspot, temperatures beneath the ridge will be higher. Therefore when examining 'temperature variations beneath ridges' there is no justification for excluding those variations that can be attributed to hotspots, nor for excluding coldspots. Ridges sample the underlying mantle—what range of temperatures and compositions is observed by this sampling?

Back-arc basins

The third set of distinctive ridges is associated with back-arc basins. Here the contrast with the global population of ridges is most pronounced. BAB segment average compositions have low TiO_2 and FeO, as noted by Taylor & Martinez (2003), and high SiO_2 and Al_2O_3. They form almost completely separated fields on many diagrams (see Fig. 7). Part of this major element signal may be due to the higher water contents in BAB magmas, which tend to suppress the crystallization of plagioclase. Delayed plagioclase could lead to lower FeO and higher Al_2O_3 values at MgO = 8 wt %; we have attempted to correct for this effect by delaying the kink associated with plagioclase appearance based on the data distribution in the segments. The more detailed evaluation by Langmuir *et al.* (2006*a*) pointed out that plagioclase suppression could not be the

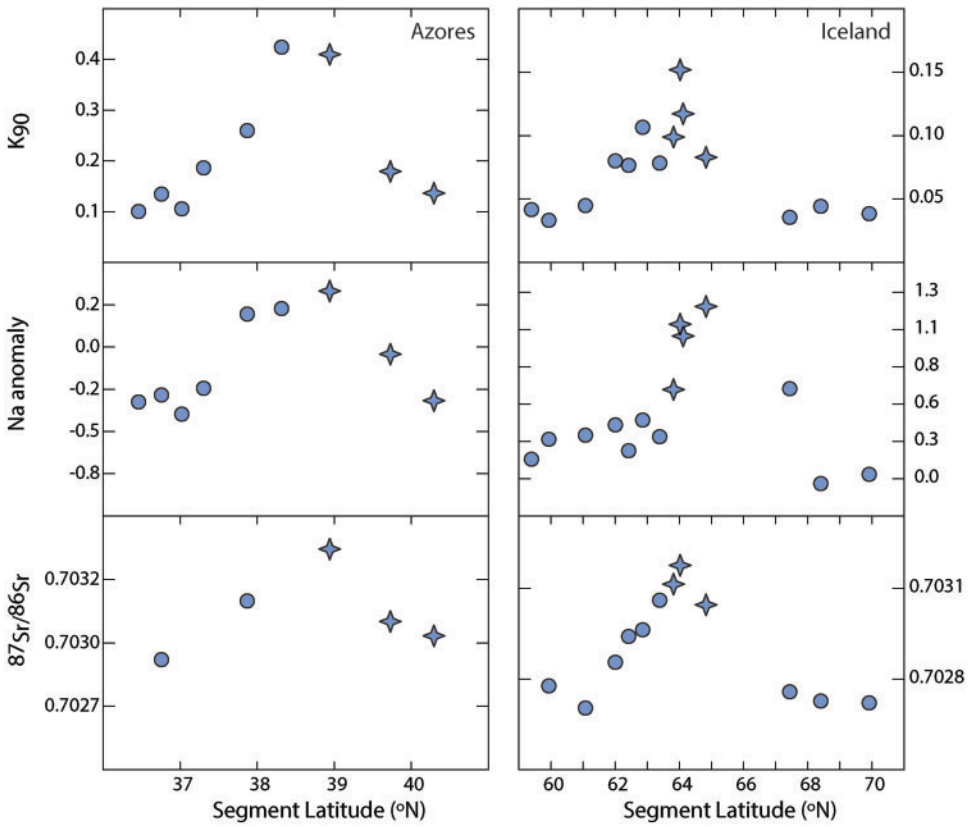

Fig. 15. K_{90}, 'Na anomaly' and $^{87}Sr/^{86}Sr$ vs segment latitude for transects near the Azores and Iceland plumes. Data for $^{87}Sr/^{86}Sr$ are from Gale *et al.* (2013*a*); symbols as in previous figures. Na anomaly is calculated as the difference between the observed and 'predicted' Na based on the correlation between $Na_{8\cdot0}$ and ridge depth apparent in open-ocean ridges away from plumes. The pronounced increase in Na_2O, K_2O and $^{87}Sr/^{86}Sr$ near the plume should be noted. The observed enrichment is probably related to a localized influence of source heterogeneity.

sole cause of the distinctive BAB signature. The existence of this signature—and the fact that it becomes even more pronounced if the effects of water are not taken into account—holds the promise of permitting identification of the tectonic setting of ophiolites through Earth history. It also suggests that fundamental aspects of melt formation and transport at back-arc ridges differ from those for open ocean ridges (Langmuir *et al.*, 2006*a*).

Another distinction of BAB segments is their offset in $Na_{8\cdot0}$–$Ti_{8\cdot0}$. Langmuir *et al.* (2006*a*) demonstrated that this offset could be explained by source depletion (leading to low TiO_2) followed by source enrichment that added Na_2O but not TiO_2. Such events would be consistent with a back-arc environment where the complex flow field in the mantle wedge could lead to source depletion, and materials coming from the down-going slab could lead to the enrichment of Na_2O.

DISCUSSION

A primary aim of this study is the presentation of a global dataset that can be widely used to address and test diverse hypotheses related to the origin of MORB and their relationships to physical properties of ocean ridges, melt transport, mantle temperature, and mantle composition. For these purposes it is important to have agreement on the overall characteristics of the data. In their alternative study of the global variations of MORB and their origin, Niu & O'Hara (2008) called into question the overall systematics of MORB data. They further argued that variations in mantle composition were a primary control on ridge depth and ocean crust composition for the entire range of ridge depths, from <1000 m to >5000 m. Because the characteristics of the data are the ground truth on which interpretations must be based, the first item to address prior to considering various hypotheses for the origin of the variations is the reason for discrepancies in fundamental data description between this study and that of Niu & O'Hara (2008).

Comparison between this study and that of Niu & O'Hara (2008)

Niu & O'Hara (2008) contended that the global 8-value correlations disappear if normalization is made to Mg# 72 (equivalent to our Fo_{90} values). Because in the treatment above there is no evidence supporting this assertion, it is

necessary to explore in detail the causes of the discrepancies between these two studies.

The key difference between the results of Niu & O'Hara (2008) and the present results is that the former show a change of only 1 wt % FeO with axial depth in contrast to the ~5 wt % FeO change with axial depth shown here. Niu & O'Hara (2008) suggested the correction to 8 wt % MgO is the source of the discrepancy. Yet the mean Fe_{90} values presented here, equivalent to the Mg# 72 values of Niu & O'Hara (2008), confirm the global range of over 5 wt % FeO, and the data correlate inversely with axial depth, Na_{90} and Al_{90}. Careful examination of the procedures of Niu & O'Hara reveals the differences between the two studies. Although there are three important differences, the key difference that leads to the contrasting conclusions lies in their methods of fractionation correction.

Contrast 1: data selection and coverage

The major element dataset used in this study (Gale *et al.*, 2013*a*) includes large quantities of previously unavailable data from regions such as the PAR, Gakkel Ridge and Central Indian Ridge (CIR), and care was taken to ensure a high-quality database. Inter-laboratory bias correction factors were applied to 92% of the data and all data were normalized to constant sums taking into account volatile contents. The full dataset of raw and corrected data is available (Gale *et al.*, 2013*a*; Supplementary Data). In contrast, Niu & O'Hara (2008) downloaded raw data from PetDB and eliminated samples erupted shallower than 400 m, with SiO_2 >53 wt % or MgO <7 wt %, or without water depth information. Niu & O'Hara do not appear to have eliminated duplicates, dealt with inter-laboratory bias issues, or removed off-axis samples. The data file was not made available, thereby precluding any knowledge of the geographical locations of the samples or the major element composition of the samples used in their calculations. With our dataset, however, using their procedures it is possible to reproduce the essence of their results. Neither the amount and quality of data used, nor the different screens that were applied to the two datasets, are the primary cause of the discrepancies.

Contrast 2: calculation of ridge depth

The mean depth of each segment in the Gale *et al.* (2013*a*) catalog is calculated using the digital output from GeoMapApp (Ryan *et al.*, 2009), which consists of evenly spaced points with depth information along the length of each segment. Niu & O'Hara (2008) used instead the actual sample eruption depths and bin, irrespective of geographical location, all samples from specific depth intervals (such as 3000–3250 m). Some of these samples may be far from their eruption depth, for example if they are from rift valley walls. All information about location, spreading rate, and regional depth is thereby eliminated from the Niu & O'Hara approach.

Binning by sample recovery depth leads to the following problems. The goal of a global study is to assess the effect of large-scale variables such as mantle temperature and mantle composition on the diversity of erupted basalts. Because of the rapid diffusion of heat, mantle potential temperature varies on scales of >~100 km. For example, using a thermal diffusivity of $8 \times 10^{-7}\,m^2\,s^{-1}$ (Katsura, 1995), temperature homogenizes over 20 km in only 20 Myr, a fraction of the opening time of an ocean basin. Therefore, 'regional depth', reflecting the mean depth of the region, is the appropriate parameter to use when exploring variables such as mantle temperature. Indeed, within a given ridge segment, particularly at slower spreading rates, tectonic processes can lead to >1000 m of depth variation over distances of kilometers that have nothing to do with the temperature of the mantle. Niu & O'Hara (2008) binned basalts that may have erupted within a few kilometers of each other, perhaps from the rift valley floor and rift valley walls, or segment centers versus segment ends, into different depth bins. These samples nonetheless must be derived from mantle with the same potential temperature. Also, basalts erupting from ridges located at opposite sides of the globe could be placed in the same depth bin, ruling out any possibility of evaluating regional variations. For example, if the method of Niu & O'Hara (2008) is used to bin the Gale *et al.* (2013*a*) dataset by sample eruption depth, the 1500–1750 m bin contains samples from more than five ridges, some of which have regional depths far from these values. The advantages of the mean segment depth adopted here are that it smooths out the depth variations related to local tectonic effects, is a parameter sensitive to mantle potential temperature and regional mantle composition, and allows a global comparison based on geography, spreading rate, or other parameters.

To investigate the consequences of the binning approach, the current dataset was binned using sample recovery depth and the same depth intervals as used by Niu & O'Hara (2008), eliminating samples with depths <400 m for consistency with their study. Figure 16 shows the large discrepancies in depth that their approach can cause. From Fig. 16 it is evident that the bins at deep sample depths include segment depths that are much shallower, and many sample depths of <3000 m come from segment depths that are much deeper. As there are correlations between segment depth and chemical parameters (Fig. 6), binning deep samples into shallow bins and shallow samples into deep bins lessens the overall range of the data.

Despite the shortcomings of the binning method, this effect is not the major factor in the differences between the two studies. Figure 17, which uses the Niu & O'Hara (2008) approach on our dataset, shows that the binning method (and the exclusion of Iceland) limits the total range of variation. Nonetheless, the ~3·5 wt % variation

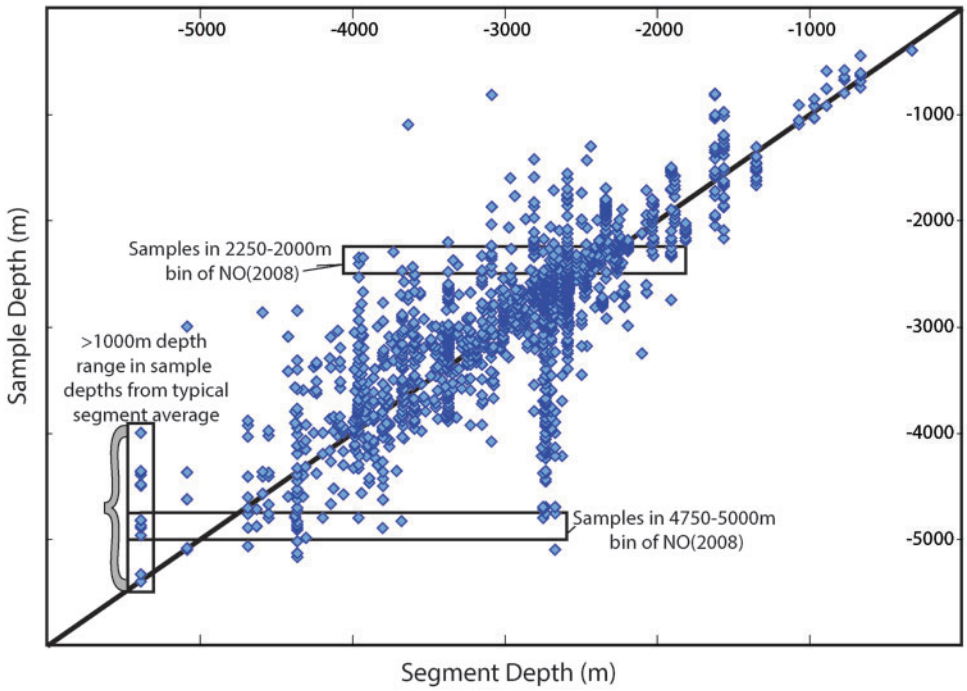

Fig. 16. Sample recovery depth vs mean segment depth for basalts in this study. It should be noted that, from a given segment, sample recovery depths can vary by 1000 m or more (see vertical box). This variation is primarily related to the structural characteristics of ridge segments; for example, samples can be recovered from the rift valley and its walls. Sample recovery depth reflects local tectonics and is not the appropriate measure for comparison with large-scale mantle properties of composition or temperature. The horizontal boxes show the samples that would be binned in a single depth interval by the procedure of Niu & O'Hara (2008) [NO(2008)], coming from segments with mean depths that can vary by 2000 m.

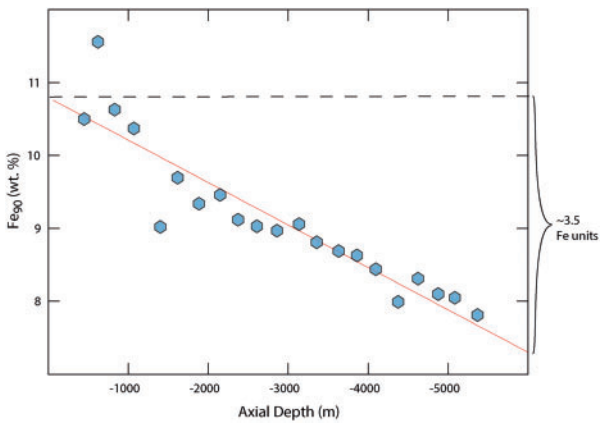

Fig. 17. Fe_{90} vs axial depth, calculated using the depth-binning technique advocated by Niu & O'Hara (2008). Sample 90-values determined in this study were binned by sample recovery depth following the protocol of Niu & O'Hara (2008), including the exclusion of samples recovered from shallower than 400 m. This technique reduces the global variation in Fe_{90} from ~5 to 3·5 wt %, but the overall trend of decreasing Fe_{90} with increasing ridge depth remains.

in FeO from adopting the Niu & O'Hara (2008) binning approach is still far more than the 1 wt % variation they claimed [see fig. 10 of Niu & O'Hara (2008)]. Although binning by sample depth does diminish the total range of observations, it cannot be the major reason for the discrepancies in results.

Contrast 3: method of fractionation correction

The most important difference between the two studies is the method of fractionation correction. As discussed at length above, the data treatment in this study uses fractionation correction methods based on LLD that are calibrated to experimental data, and checked against the data from each segment. Niu & O'Hara (2008) instead followed the approach of Niu *et al.* (1999), and applied a global data correction based on data from a limited region, largely the EPR, that was fitted with a sixth-order polynomial. Niu & O'Hara (2008) updated the MgO and FeO calibration using a second-order polynomial fit to their global dataset. The second-order polynomial fit for MgO and FeO leads to odd behavior—for example, a sample that has its MgO and FeO contents corrected to a given Mg# using their polynomial has corrected MgO and FeO contents that do not reproduce the Mg# to which they were corrected. The discrepancy gets larger as the magnitude of the correction increases, so that samples with MgO near 7 wt % can have corrected Mg#'s of <70.

A flaw in a polynomial correction scheme is that LLD are not polynomial functions. For MORB, LLD are quasi-linear line segments with abrupt kinks where a new phase appears on the liquidus. For many elements

(e.g. MgO, Na_2O, TiO_2) the change in concentration is unidirectional with decreasing temperature (for MORB with >5% MgO). There is no change in the sign of the slope, and as long as a particular phase assemblage is crystallizing the slopes on variation diagrams are close to linear. There is no thermodynamic or other justification for a polynomial correction scheme, which inherently has changes in the sign of the slope, and no regions of constant slope. These functional characteristics are not those of LLD pertinent to oceanic basalts. These drawbacks are illustrated in Fig. 18, which shows the polynomial expressions for MgO and FeO used by Niu & O'Hara (2008) for fractionation correction. It should be noted that along each polynomial curve MgO first decreases and ultimately increases with decreasing Mg#.

For samples that have 8–9 wt % FeO, where Niu & O'Hara (2008) calibrated their polynomial, the errors imposed by their approach are small. The polynomial has a shallow slope around MgO = 9 wt %, where olivine crystallizes alone, and then it steepens between 8·5 and 7 wt % MgO, where plagioclase (and possibly cpx) are also crystallizing. Where the errors become significant is when the same polynomial is used to correct samples with higher or lower FeO contents (Fig. 18). The Niu & O'Hara procedure simply translates the polynomial along a line of constant Mg/(Mg + 0·9Fe). This causes the same curvature independent of FeO (and hence MgO content). Samples with high MgO and FeO have the same curvature as samples with low MgO and FeO with the same Mg#. Because the curvature reflects plagioclase appearance, the high curvature associated with 'plagioclase-in' moves erroneously to higher MgO as FeO increases. High-FeO samples have a steep correction slope at high MgO, whereas low-FeO samples have a steep correction slope only at very low MgO. The consequence is that high-FeO samples are over-corrected, and low-FeO samples are under-corrected, thus compressing (inaccurately) the range of Fe_{90} [called Fe_{72} by Niu & O'Hara (2008)]. It should be noted that this feature of their procedure is a numerical artifact of their polynomial approach.

This phenomenon is illustrated in Fig. 18, where LLD are shown for high- and low-FeO magmas and compared with the Niu & O'Hara (2008) polynomials and the '72 values' from their correction scheme. Note that one cannot simply backtrack along the dashed polynomials, because their correction does not actually correct the data to a Mg# of 72, but to variable Mg#'s near 72. Example '72 values' for the ends of the LLD shown in thick solid lines in the figure are indicated by the open stars. The 72 value for the middle LLD in the figure gives the correct value at Mg#72, but the high FeO sample is corrected far too low, and the low FeO sample far too high. Therefore, the Niu & O'Hara (2008) correction scheme is not generally applicable to the range of MORB compositions.

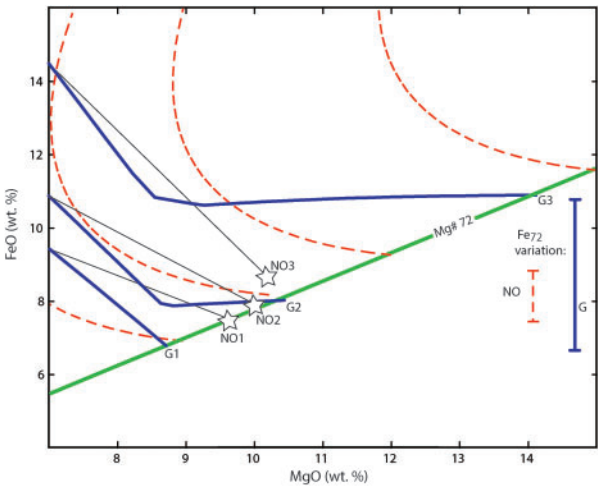

Fig. 18. FeO vs MgO (wt %) comparing calculated LLD (continuous lines) with the polynomials used by Niu & O'Hara (2008) (dashed lines), which they used to correct for fractionation back to Mg# 72 (equilibrium with mantle olivine). All corrected values using this method should lie on the continuous line labeled Mg# 72, but in practice the Niu and O'Hara method corrects to a range in Mg#. For this reason, the dashed polynomials cannot be used to strictly backtrack data. It should be noted that corrections based on LLD have a flat slope while olivine only is crystallizing, and then a steep slope once plagioclase has joined the liquidus near 8·5 wt % MgO. At moderate FeO contents between 9 and 10 wt %, in the chemical range where the Niu & O'Hara (2008) polynomial was calibrated, the two corrections are similar. At higher FeO contents, however, the Niu & O'Hara (2008) polynomials have a steep slope, similar to the 'plag in' slope, at very high MgO where plagioclase cannot be stable. This over-steepened slope at high MgO contents results in an over-correction of high-FeO magmas to low FeO values at Mg# 72. For example, a lava with 7 wt % MgO and 14 wt % FeO would track line G3 to have Fe_{72} of 11 wt % using an LLD, but would correct to the star labeled NO3 to have Fe_{72} of 8.76 wt % using the polynomial correction. The opposite problem occurs for low-FeO magmas. A composition with 7 wt % MgO and 8 wt % FeO would be corrected using an LLD along the same slope as line G1 to have an Fe_{72} of 6·5 wt %, whereas the polynomial correction leads to the star labeled NO1 with Fe_{72} of 7.41. The over-correction for high-FeO magmas and under-correction for low-FeO magmas leads to an erroneous compression of real variations of FeO content in parental magmas, as indicated in the bars on the right of the diagram.

Some simple numerical examples illustrate the flaws in the polynomial scheme. To arrive at an Fe_{72} value of 11%, for example, the polynomial fit would require a lava to have 20 wt % FeO at 8 wt % MgO. No terrestrial lava has such a composition, but mantle melts with 11 wt % FeO are evident both in natural samples and in experimental data. Also, samples with 7·5% MgO and anywhere from 10 to 16% FeO produce Fe_{72} values which range in Mg# from 68 to 71.4. If they were actually corrected back to Mg# of 72, they would all have approximately the same Fe_{72} contents.

To demonstrate further that this is the source of the discrepancy between the two studies, samples from five ridge segments in our dataset were selected that span a range of

axial depths and FeO contents. To be consistent with the approach of Niu & O'Hara (2008), samples with MgO <7% were excluded. Each sample was then corrected to equilibrium with mantle olivine using both the Niu & O'Hara (2008) polynomial approach and the approach in this study. The 90-values for each segment resulting from the two correction methods, calculated using identical samples, can then be readily compared. Figure 19 shows the large discrepancy between the Fe_{90} values for high-FeO segments estimated using the Niu & O'Hara (2008) polynomial versus the LLD method used here. The higher the FeO contents in the original magmas, the larger the lowering of the Fe_{90} content by the polynomial. This explains why real global variations in Fe_{90} of multiple weight per cent are reduced to almost nothing in the Niu & O'Hara (2008) study. The errors are similarly large for Al_2O_3. It should be noted that the issues evident in FeO and Al_2O_3 are less important for Na_2O, as the segment means are relatively comparable (Fig. 19). For Na_2O the change in slope when plagioclase appears relative to olivine is smaller, so the correction errors are smaller.

The conclusions from this analysis are as follows.

(1) The Niu & O'Hara (2008) correction scheme should not be used for fractionation correction. Polynomials are an incorrect functional form, and extrapolation of a polynomial function outside its precise range of calibration leads to serious errors.
(2) Once the corrections are done properly, there are no discrepancies between the results for data from Niu & O'Hara (2008) and the present study.
(3) It is immaterial whether corrections are made to a constant MgO content, or a constant Mg#, or to equilibrium with some forsterite content. All of these are equivalent provided care is taken with the phase equilibria and LLD. For this reason one sees similar ranges and systematics in the 8-values and 90-values reported here. The systematics of MORB data at both 8 wt % MgO and Fo_{90} reflect real variations in the lavas and parental magmas that form the ocean crust. The next step is then to consider various hypotheses for the origin of these variations, and see to what extent these can be rigorously evaluated.

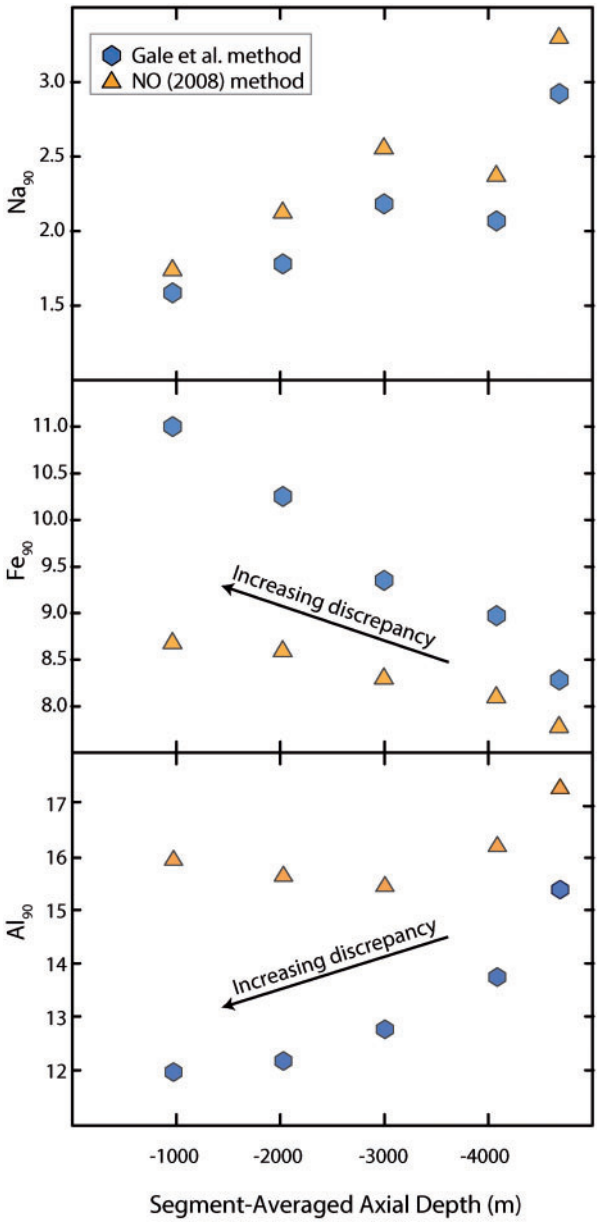

Fig. 19. Na_{90}, Fe_{90} and Al_{90} vs axial depth calculated for five segments over a large range of axial depths and chemical contents, comparing the different fractionation correction techniques in this study and in that of Niu & O'Hara (2008) [NO(2008)]. The axial depth shown is segment-averaged axial depth. It should be noted that the mistaken lowering of the high FeO contents when using the Niu & O'Hara (2008) polynomial causes increasing disparity of up to almost 2·5 wt % in the calculated Fe_{90} values. A similar disparity is seen in the calculated Al_{90} values. Because Na is an incompatible element much less sensitive to the exact crystallization sequence, the two studies track each other much more closely in Na_{90}.

Hypotheses for the origin of the global systematics of MORB

There have been several hypotheses presented to account for global MORB data: mantle temperature, mantle composition, thickness of the overriding lithosphere, and melt–rock reaction during melt transport. Of course, all of these aspects will be important to a greater or lesser degree. At superslow-spreading centers, all thermal models show the importance of a thicker lithosphere (Reid & Jackson, 1981; Bown & White, 1994). At BAB, water content (Stolper & Newman, 1994; Taylor & Martinez, 2003; Kelley *et al.*, 2006; Langmuir *et al.*, 2006*a*)

and mantle heterogeneity (Langmuir *et al.*, 2006*a*) are important features. Many hotspots show clear evidence for heterogeneity of various kinds (e.g. Langmuir *et al.*, 1992; Asimow & Langmuir, 2003; Dick *et al.*, 2003; Sobolev *et al.*, 2011). Additionally, melt–rock reaction seems an inevitable aspect of melt transport (e.g. Collier & Kelemen, 2010). Although all of these probably contribute to the variations seen in MORB, there is lack of agreement on the relative importance of the various factors. (1) Klein & Langmuir (1987), Langmuir *et al.* (1992, 2006*a*) and Asimow & Langmuir (2003) interpreted the data primarily in terms of mantle temperature variations, with important effects for mantle heterogeneity associated with some hotspots, for H_2O in back-arc basins and at some hotspots, and for thicker lithosphere at superslow-spreading ridges. (2) Shen & Forsyth (1995) proposed limited temperature variation, and that the primary control was the thickness of the lithospheric lid coupled with mantle heterogeneity. (3) Niu & O'Hara (2008) proposed an effect dominated by mantle composition. In their hypothesis, deep ridges are underlain by more fertile mantle, and shallow ridges by more depleted mantle. (4) Kimura & Sano (2012) suggested that all variations could be accounted for by melt–rock reaction. All of these studies used different datasets and correction methods, which makes quantitative comparison difficult. A primary purpose of this study and that by Gale *et al.* (2013*a*) is to provide a carefully corrected and comprehensive global dataset that can be used to address these various hypotheses from a common data platform. Inclusion of trace element data (Gale *et al.*, in preparation) will be an important additional aspect that was not included comprehensively in any of these previous studies. A definitive analysis of all the models is a larger task than can be completed here, but preliminary interpretations are provided below.

Mantle temperature vs mantle composition

To explore how well mantle temperature and mantle composition can be distinguished from one another, models that incorporate a homogeneous source composition with varying temperature can be compared with models with homogeneous temperature and varying source. Which of these best corresponds to the trends of the global 90-values? The first question is the nature of the source variations. Here we address first source variations related to the addition and subtraction of melt from the source region. Such variations are consistent with the characteristics of element variations in alpine peridotites (e.g. Frey *et al.*, 1985), with extraction of melt at ridges creating basaltic and depleted mantle reservoirs, and with the potential for recycled ocean crust to be present in variable abundance in the mantle. These variations would then range from depleted peridotites with low Na_2O, Al_2O_3 and TiO_2 and high Mg#, to fertile peridotites with high Na_2O, Al_2O_3 and TiO_2 and low Mg#.

Langmuir *et al.* (1992) explored this question for the elements Na_2O, MgO and FeO, but not for the elements Al_2O_3, CaO and SiO_2. They demonstrated that mantle temperature best explains the observed data arrays, and calculated mantle heterogeneity trends in $Na_{8\cdot0}$–$Fe_{8\cdot0}$ that are orthogonal to the data. Asimow *et al.* (2001) expanded this exploration by making calculations using the MELTS program that included all the elements. They also found an orthogonal relationship between temperature and composition for Na_2O and FeO, but noted that using MELTS, temperature variations were not entirely consistent with the MORB dataset. Here we explore these questions further by including calculations from the thermodynamic program pMELTS (Ghiorso *et al.*, 2002), from the calculations based on the methods of Langmuir *et al.* (1992) as modified by Asimow & Langmuir (2003) and Katz *et al.* (2003), and from more recent experimental data. This comprehensive approach permits a consideration of the elements Al_2O_3, CaO and SiO_2, and of how robust relationships are using the different methods. An important aspect of any comparison is the need to fit the correlation between Fe_{90} and Al_{90}, which is such a pronounced feature of the global dataset.

pMELTS has certain known issues when modeling mantle melting. In particular, pMELTS does not correspond to mantle melting experiments for several elements, such as Na_2O (Asimow *et al.*, 2001), and has other peculiarities, leading, for example, to very large changes in FeO and SiO_2 contents with mantle temperature, and a relationship between extent of melting and temperature that is inconsistent with experimental data (see Langmuir *et al.*, 2006*a*). There should thus not be undue emphasis on whether pMELTS calculations 'fit' the observations, nor on the specific temperature range observed. Nonetheless, in terms of the overall trends produced by temperature and compositional variations, pMELTS provides useful indications.

To estimate the effects of variable temperature and constant source, pMELTS pooled melt compositions [see Langmuir *et al.* (1992) for an explanation of 'pooled melt'] were calculated with mantle potential temperatures from 1300 to 1450°C using a fixed mantle starting composition (Workman & Hart, 2005). These results can be compared with pooled melt compositions calculated using a variable starting composition at a fixed mantle potential temperature of 1350°C. In the latter case, the source was varied to include (1) residual compositions from Baker & Stolper (1994), thereby showing the effects of a progressively depleted source, and (2) more enriched sources akin to different proportions of recycled crust by mixing normal (N)-MORB (Gale *et al.*, 2013*a*) in various proportions to the starting mantle composition of Baker & Stolper (1994). The results of these calculations are highlighted in Fig. 20.

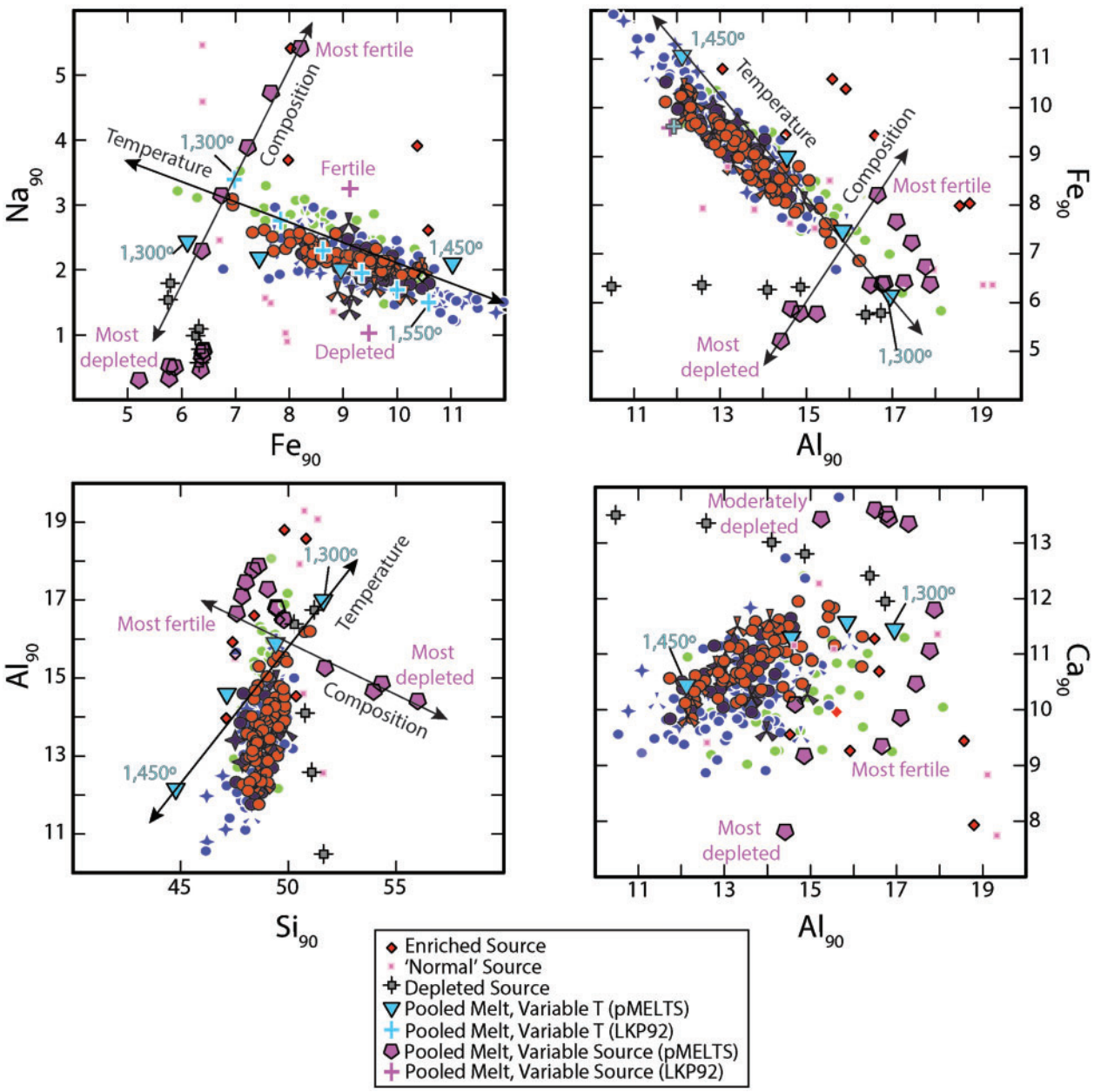

Fig. 20. Na_{90} vs Fe_{90}, Al_{90} vs Si_{90}, and Fe_{90} and Ca_{90} vs Al_{90}, showing the global data compared with pooled melt models and experimental compositions based on variations in mantle potential temperature at constant mantle composition, and constant potential temperature with variable mantle compositions. Diamonds are experimental melts from an enriched source (Hirose & Kushiro, 1993), small squares from a 'normal source' (Hirose & Kushiro, 1993), and small gray symbols a depleted source (Schwab & Johnston, 2001). Also shown are calculated pooled melt calculations from the thermodynamic program pMELTS (Ghiorso *et al.*, 2002). The pentagons show pooled melts of a range of mantle source compositions from residual to fertile (see text), at 1350°C. The triangles show melts of a fixed source composition (Workman & Hart, 2005), melted at variable potential temperatures. In the Na_{90} vs Fe_{90} panel, pooled melts of the Workman & Hart (2005) source using the Langmuir *et al.* (1992) method (LKP92) are also shown as crosses outlined in white [note that Langmuir *et al.* (1992) did not include Al, which is why the pooled melts are shown only for Na_{90}–Fe_{90}]. Pooled melts of a range of source compositions using the Langmuir *et al.* (1992) method are shown as crosses without white outlines. It is apparent that the trends associated with variable mantle temperature account for the global correlations far better than the vector associated with mantle heterogeneity. In many cases the mantle heterogeneity trend is orthogonal to the data array, and also does not lead to the requisite range of variation. Further evidence comes from the experimental data, where it can be seen that changing from one source to another results in a vector perpendicular to the global array. Mantle temperature variations of the order of ~200°C can account for the broad-scale features apparent in the global major element data.

Variations from pMELTS with mantle temperature are shown as triangles, whereas variations with composition are shown by the pentagons. For Na_{90}–Fe_{90}, and Al_{90}–Fe_{90}, the temperature and composition trajectories are roughly orthogonal. Pooled melts from variable mantle composition cross the MORB values at a high angle. Variations in mantle temperature closely follow the MORB values, except for Na_{90}, which for these conditions do not vary sufficiently in pMELTS calculations (Fig. 21). Si_{90}–Al_{90} also shows an orthogonal relationship between temperature and composition variations. In this case, the too large Si_{90} variations produced by pMELTS are also evident. Although the pMELTS calculations cannot be used for reliable estimates of temperature and have systematic errors for some elements, they clearly indicate that variations with mantle temperature more closely correspond to the MORB values, and that variations in mantle composition are inconsistent with the primary trend of the observations. Furthermore, the discrepancies between the pMELTS calculations and MORB are consistent with known problems in the pMELTS output.

Calcium is an element with a limited range of variation, and with variable behavior during melting depending on whether cpx is present. This leads to small variations in Ca_{90}. Nevertheless, the variation of Ca_{90} vs Al_{90} (Fig. 20) shows that the melting trajectory is also more consistent with the effect produced by variable mantle temperature than with that produced by variable mantle sources.

An independent line of evidence comes from comparison with experiments on mantle melting. Although these experiments are isobaric and therefore not quantitative comparisons with polybaric melting beneath ridges, they at least can show the trends of the data with varying source composition. Three sets of experiments on variably enriched sources are shown in Fig. 20. For Fe_{90}–Na_{90} and Fe_{90}–Al_{90} the array from fertile to depleted is consistent with effects of composition on the basis of the pMELTS calculations.

The orthogonal slopes produced by mantle temperature and mantle composition for FeO–Na_2O and FeO–Al_2O_3 can also be understood qualitatively. More fertile sources have higher FeO contents, and also have a lower solidus temperature, which deepens the initial pressure of melting. As shown by Langmuir & Hanson (1980), a higher FeO source leads to higher FeO melts for the same pressure and extent of melting. Higher-pressure melts also have higher FeO contents, so the two effects amplify melt FeO contents. These effects are moderated by the fact that higher alkalis lower the FeO contents of melts (Langmuir *et al.*, 1992). For Na_2O, more enriched sources have more Na_2O, which increases the Na_2O concentration in the melt, but they also melt more, which dilutes the Na_2O concentration. Doubling Na_2O in the source would require a doubling of the extent of melting to produce the same melt Na_2O content. Experimental data suggest that the melting effect is far smaller than that (Baker & Stolper, 1994; Hirschmann *et al.*, 1998). Furthermore, an important energy sink during melting is the heat of fusion, which limits the increase in extent of melting possible with more fertile sources during adiabatic upwelling. The increase in extent of melting thus does not offset the source change, so that more Na_2O-rich sources produce melts with higher Na_2O contents. For Al_2O_3, the relative change in source composition is smaller than for Na_2O, so enriched sources produce melts with only slightly higher Al_2O_3. Source heterogeneity thus creates large increases in Na_2O and small increases in Al_2O_3 as FeO increases slightly. These are not the variations observed in MORB data.

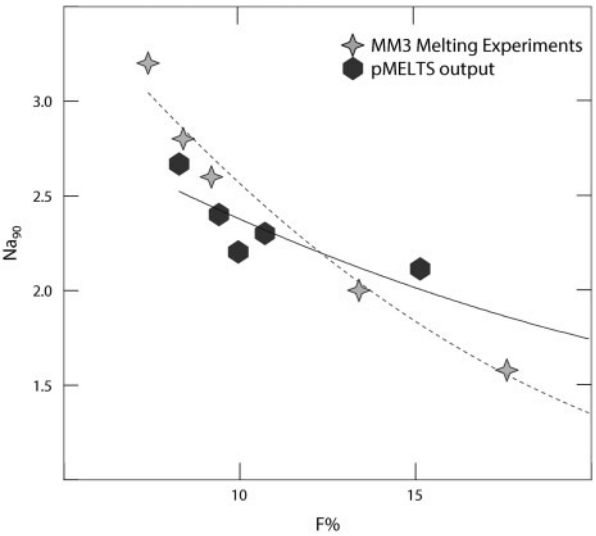

Fig. 21. Na_{90} vs degree of melting F% for experiments on mantle composition MM3 (Baker & Stolper, 1994; Hirschmann *et al.*, 1998) compared with the output from pMELTS. Lines are best-fit polynomials. The Na_{90} in the pMELTS output is slightly too low at low extents of melting, and much too high at higher extents of melting relative to the experiments, leading to a diminished range of predicted Na contents.

A quantitative assessment can be made using the calculations of Langmuir *et al.* (1992), which are based on experimental partitioning data and have been shown to reproduce accurately experimental results for a variety of compositions (e.g. Baker & Stolper, 1994; Wasylenki *et al.*, 2003). Results for Na_{90}–Fe_{90} are shown in Fig. 20. The results for fractional melting of the mantle composition of Workman & Hart (2005) with 150 ppm water water at different potential temperatures correspond closely to the MORB 90-values. Most of the MORB data plot between mantle potential temperatures of 1325 and 1525°C. Calculations of variations in mantle composition produce trends orthogonal to temperature variations, in qualitative agreement with pMELTS calculations, and inconsistent with the principal component of the data (Langmuir *et al.*, 1992).

All of the above evidence refutes the hypothesis that the principal component of variations in MORB compositions is produced by variations in mantle fertility associated with varying amounts of a basaltic component in the mantle source. Calculations with pMELTS, the independent calculations of Langmuir *et al.* (1992), and the raw experimental data are all consistent with one another. Mantle depletion and fertility are associated with a wide range in Na_2O and Al_2O_3 with little change in FeO, and these systematics are orthogonal to the principal component of the MORB data. The discrepancy is not limited to FeO, however. Si–Al and Ca–Al variations lead to the same conclusions. These observations suggest that a primary influence on MORB chemistry is mantle temperature, which appears to vary over ~200°C based on the calculations in this study.

Mantle heterogeneity is, of course, obvious and necessary once one considers the more highly incompatible elements. The range in K_{90}, for example, by a factor of 50, is far more than can be accounted for by melting variations, and must relate to source heterogeneity. This is further supported by the fact that K_{90} correlates roughly with radiogenic isotopes. As noted above, there is also a pronounced deviation in Na_2O concentration as a function of depth when hotspots are approached. Hotspots have higher $Na_{8\cdot0}$ or Na_{90} than other ridges at the same depth, suggesting either an offset to shallower depths owing to active upwelling, or a change in mantle source composition. The exceptionally low Fe_{90} of the segments near the Azores plume has also been explained in terms of major element heterogeneity associated with the plume (Langmuir & Hanson, 1980; Schilling *et al.*, 1980). There is little doubt that mantle heterogeneity has a significant effect on basalt major element compositions in some regions. One form of such heterogeneity, for example, would be the metasomatism of a major element depleted source by a low-degree melt enriched in incompatible elements (Gale *et al.*, 2011). This could lead to low FeO and high K_2O contents, which is characteristic of some portions of the ridge system.

Is it reasonable that for most of the ridge system, major element compositions show relatively little variation, whereas incompatible elements such as K show large variations? It is if the origin of mantle heterogeneity is very low-degree melts (e.g. Plank & Langmuir, 1993; Halliday *et al.*, 1995; McKenzie & O'Nions, 1995; Donnelly *et al.*, 2004; Rudge *et al.*, 2005; Gale *et al.*, 2011). Low-degree (low-*F*) melts have a large influence on trace elements, but little effect on major elements. For example, at high pressures where low-*F* melts are generated, the bulk partition coefficient (*D*) for Na is elevated owing to the increased jadeite component in residual cpx, reaching values of about 0·1. Elements such as Th, Ba, U and K, however, have *D* values of about 0·001. Deep, low-*F* melts can then be enriched by a factor of 100–1000 in highly incompatible trace elements, but by only a factor of 10 in Na_2O. With a typical source concentration of ~1 ppm Ba and 0·22 wt % Na_2O (Langmuir *et al.*, 1992; Salters & Stracke, 2004), a low-*F* melt might have 500 ppm Ba and 2·2 wt % Na_2O. Adding 1% of this melt to a depleted mantle then raises the source Ba content by a factor of six, but increases the source Na_2O by only 18%. This is an 'enriched' mantle in terms of trace elements, but the major elements would show little effect.

The same logic holds true for the depletion of the mantle; extraction of a 2–3% mantle melt severely depletes the incompatible element concentrations of the source with minimal impact on the major elements. For an incompatible element with a *D* of 0·001, for example, the residue can be depleted by 95% by the extraction of a 2% melt, whereas major elements are diminished by less than 10% (Gale *et al.*, 2011). These results reconcile the apparent conflicting signatures between trace elements and major elements, and are not in conflict with mantle temperature variations beneath ridges.

Reactive crystallization

Collier & Kelemen (2010) have made a case for reactive crystallization as an important process for MORB petrogenesis to account for variations on the <50 km scale. Kimura & Sano (2012) have suggested that this process can also account for the global variations of MORB. Kimura & Sano (2012) used the correction scheme of Niu & O'Hara (2008), however, and thus their modeling does not accurately reflect the variations at ocean ridges. Collier & Kelemen (2010), however, carefully binned their samples on a segment scale similar to Gale *et al.* (2013*a*), and performed quantitative modeling using pMELTS to explore the possible consequences of reactive crystallization.

Reactive crystallization within the mantle is able to change melt mass and chemical composition at constant Mg#. Because it is a process that inevitably takes place with declining pressure, the effect is to move melt compositions along a line of constant Mg# to lower FeO values as pressure decreases. Because the dominant reaction involves the precipitation of lower-SiO_2 olivine and dissolution of higher-SiO_2 orthopyroxene, as FeO declines, SiO_2 increases. The other elements are largely controlled by melt mass and the extent to which cpx precipitates from the melt. If melt mass goes down, the more incompatible elements such as Na_2O, TiO_2 and Al_2O_3 increase. If precipitation of cpx occurs, CaO contents can decrease, lowering the ratio of $Ca/(Ca + Na)$. In principle, then, this can produce qualitatively important aspects of the global variability—the negative correlation between FeO and SiO_2, and, if melt mass changes in exactly the right way, the corresponding increases in Na_2O, TiO_2 and Al_2O_3.

There are physical predictions of how such changes should correlate with the tectonic variables of the ridge

system, such as spreading rate. As pointed out by Langmuir *et al.* (1992), and re-emphasized by Collier & Kelemen (2010), the variance of most variables increases with decreasing spreading rate. At slow spreading rates, ridges can be subaerial at Iceland and at depths of 5000 m along the Cayman Rise. $Na_{8\cdot0}$ and $Fe_{8\cdot0}$ also display their total range of variation at slow spreading rates. The fastest-spreading ridges are in contrast relatively uniform. Collier & Kelemen (2010) took these observations as supporting evidence for reactive crystallization in the production of such diversity. Instead, it could be argued that we should see a progressive change that is systematic with spreading rate. At fast-spreading ridges, where the melting regime extends to the base of the crust, there should be no reactive crystallization, and magmas should have the highest FeO and lowest SiO_2 contents. At slow-spreading ridges, magmas should be lower in FeO, higher in SiO_2 and potentially higher in Na_2O, TiO_2 and Al_2O_3 depending on the melt mass. A prediction of this hypothesis would then be that the fastest-spreading ridges would have the lowest $Si_{8\cdot0}$ and highest $Fe_{8\cdot0}$, and the slowest-spreading ridges the highest $Si_{8\cdot0}$ and lowest $Fe_{8\cdot0}$. A parameter that might reflect this phenomenon would be the Si/Fe ratio normalized to provide equal weighting for both SiO_2 and FeO [e.g. $Fe_{8\cdot0}/(Si_{8\cdot0} - 41)$]. If reactive crystallization were a controlling process, one would qualitatively predict a correlation between this parameter and spreading rate. Alternatively, the mantle temperature hypothesis predicts no correlation with spreading rate and a positive correlation with axial depth. Figure 22 shows that there is a positive correlation with axial depth, and no correlation with spreading rate. The evidence suggests, therefore, that although reactive crystallization may prove to be a significant process for explaining some of the variations between samples at the segment scale, as suggested by Collier & Kelemen (2010), it is unlikely to be a dominant process for explaining the global systematics of segment averages explored here.

Effects of lithospheric thickness

Although there is no correlation between the predictions of melt–rock reaction and lithospheric thickness, there are clear offsets in the data from the slowest-spreading ridges compared with faster-spreading ridges (Fig. 14). The hallmarks of slow-spreading ridges are lower corrected SiO_2 for the same corrected FeO, and higher corrected Na_2O and Al_2O_3 relative to FeO, SiO_2 and TiO_2. What process could lead to these differences?

During mantle melting, SiO_2 is sensitive to the mean pressure of melting, whereas FeO is more sensitive to the initial pressure of melting [see calculated curves of Langmuir *et al.* (1992)]. For this reason, during mantle upwelling beneath ocean ridges, thick lithosphere tends to decrease melt SiO_2 contents, while leaving FeO contents little changed. At the same time, thick lithosphere will decrease the extent of melting, causing Na_2O (and Al_2O_3) contents to increase. For TiO_2, the effect is complicated by the very strong temperature dependence of Ti partitioning

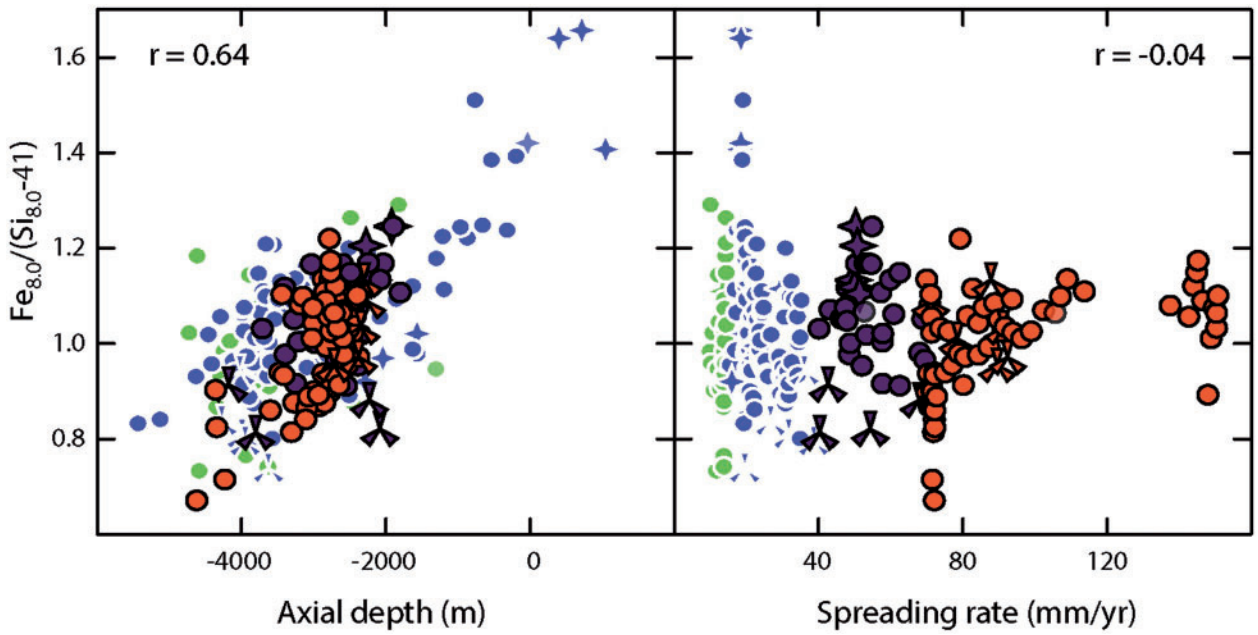

Fig. 22. $Fe_{8\cdot0}/(Si_{8\cdot0} - 41)$ vs mean depth (m) and spreading rate (mm a^{-1}). It should be noted that a robust correlation exists with mean depth, and no correlation exists with spreading rate. Melt–rock reaction is predicted to increase as spreading rate decreases, which would lead to decreasing FeO and increasing SiO_2 [lower $Fe_{8\cdot0}/(Si_{8\cdot0} - 41)$] as spreading rate decreases. As no such correlation is apparent, melt–rock reaction is probably a minor influence on global ridge basalt systematics.

shown by Kinzler (1997). For colder ridges, which are highly represented at superslow-spreading ridges, the lower mantle temperatures lead to a high partition coefficient for TiO_2, causing TiO_2 contents to go up less than would be predicted by melting models based on constant partition coefficients.

The predictions for a melting model with a thicker lithosphere are then decreased SiO_2, and increased Na_2O and Al_2O_3 relative to FeO, with muted effects for TiO_2. Qualitatively these are just the offsets that are observed in Fig. 14. Of course, higher-pressure fractionation is also likely to take place in this setting, contributing to the low CaO contents that are characteristic of the superslow ridge environment. The observations at the slowest-spreading ridges appear to be more consistent with lower extents of melting at higher pressures, coupled with high-pressure fractionation, rather than an increased role for reactive crystallization. A more extensive evaluation of this model, however, requires a fully coupled model of melt transport and associated reactive crystallization.

CONCLUSIONS

(1) Global ocean ridge basalt major element data have been corrected for fractionation to their values at 8 wt % MgO, and to equilibrium with Fo_{90} olivine, using a custom correction scheme for each of 241 ridge segments. The data include ridge segments from the full range of axial depths (+1000 to −5000 m), and from all spreading rates.

(2) The corrected values provide magma compositions for each segment that can be compared with each other with minimal effects of fractionation processes. The aim is to provide a definitive database to explore the global chemical systematics of MORB and to allow evaluation of different ridge and mantle melting models.

(3) The inter-element systematics of compositions corrected to 8 wt % MgO or to constant $Mg/(Mg + Fe)$ (i.e equilibrium with mantle olivine) are in close agreement, in contrast to claims made in the literature (Niu & O'Hara, 2008).

(4) The 8- and Fo_{90}-values show coherent global correlations with each other and with ridge depth. There is no correlation between the chemical parameters and spreading rate. In general, the standard deviation of mantle-derived physical and chemical ridge properties increases as spreading rate decreases.

(5) These data can be used to distinguish the relative importance of mantle temperature and mantle composition in generating the chemical diversity of global MORB. A mantle temperature range of ~200°C best explains the correlations. Variable fertility of mantle sources may be important regionally, but produces major element trends that are orthogonal to the principal component of the global dataset.

(6) Mantle heterogeneity also contributes to the chemical systematics, evident in the higher Na_2O contents of MORB at plume-influenced ridge segments relative to segments of the same depth distant from plumes. K, the most incompatible major element, shows broad correlations with radiogenic isotopes and a factor of 50 variation, also requiring a role for source heterogeneity. The evidence for a relatively homogeneous source in terms of major elements, and a very heterogeneous source in terms of highly incompatible elements, suggests that addition and removal of low-degree melts, not large-scale changes in mantle composition, are responsible for the mantle heterogeneity widely discussed at ocean ridges.

(7) Superslow-spreading ridge segments are offset to low CaO and SiO_2, and high Al_2O_3 and Na_2O, relative to faster-spreading ridge segments. These offsets are not predicted by models of reactive crystallization, but are instead consistent with lower extents of melting caused by a thickened lithospheric lid at the slowest-spreading ridges.

(8) Back-arc basins have distinct compositions relative to open ocean spreading centers, marked by higher Al_2O_3 and SiO_2, and lower FeO and TiO_2. These effects reflect the diverse processes of source depletion and source enrichment from the slab that occur in the back-arc environment, and the major effect of high water contents. The distinctive chemical signature of back-arc basin basalts should permit the clear recognition of back-arc spreading centers in the geological record.

ACKNOWLEDGEMENTS

This paper greatly benefited from thoughtful reviews by John Maclennan, Katie Kelley and John Sinton, and from the editorial support of Marjorie Wilson.

FUNDING

This work was supported by NSF grants OCE-0752281 and OCE-1061264.

SUPPLEMENTARY DATA

Supplementary data for this paper are available at *Journal of Petrology* online.

REFERENCES

Argus, D. F., Gordon, R. G. & DeMets, C. (2011). Geologically current motion of 56 plates relative to the no-net-rotation reference frame. *Geochemistry, Geophysics, Geosystems* **12**, Q11001, doi:10.1029/2011GC003751.

Asimow, P. D. & Langmuir, C. H. (2003). The importance of water to oceanic mantle melting regimes. *Nature* **421**, 815–820.

Asimow, P. D., Hirschmann, M. M. & Stolper, E. M. (2001). Calculation of peridotite partial melting from thermodynamic models of minerals and melts, IV. Adiabatic decompression and the composition and mean properties of mid-ocean ridge basalts. *Journal of Petrology* **42**, 963–998.

Baker, M. B. & Stolper, E. M. (1994). Determining the composition of high-pressure mantle melts using diamond aggregates. *Geochimica et Cosmochimica Acta* **58(13)**, 2811–2827.

Batiza, R. (1984). Inverse relationship between Sr isotope diversity and rate of oceanic volcanism has implications for mantle heterogeneity. *Nature* **309**, 440–441.

Bender, J., Langmuir, C. & Hanson, G. (1984). Petrogenesis of basalt glasses from the Tamayo region. *Journal of Petrology* **25**, 213–254.

Bird, P. (2003). An updated digital model of plate boundaries. *Geochemistry, Geophysics, Geosystems* **4**, 1027, doi:10.1029/2001GC000252.

Bown, J. W. & White, R. S. (1994). Variation with spreading rate of oceanic crustal thickness and geochemistry. *Earth and Planetary Science Letters* **121**, 435–449.

Collier, M. L. & Kelemen, P. B. (2010). The case for reactive crystallization at mid-ocean ridges. *Journal of Petrology* **51(9)**, 1913–1940.

Danyushevsky, L. V. & Plechov, P. (2011). Petrolog3: Integrated software for modeling crystallization processes. *Geochemistry, Geophysics, Geosystems* **12**, Q07021, doi:10.1029/2011GC003516.

DeMets, C., Gordon, R. G., Argus, D. F. & Stein, S. (1994). Effect of recent revisions to the geomagnetic reversal timescale on estimates of current plate motions. *Geophysical Research Letters* **21(20)**, 2191–2194.

Dick, H. J. B., Lin, J. & Schouten, H. (2003). An ultraslow-spreading class of ocean ridge. *Nature* **426(6965)**, 405–412.

Donnelly, K. E., Goldstein, S. L., Langmuir, C. H. & Spiegelman, M. (2004). Origin of enriched ocean ridge basalts and implications for mantle dynamics. *Earth and Planetary Science Letters* **226(3–4)**, 347–366.

Dungan, M. A. & Rhodes, J. M. (1978). Residual glasses and melt inclusions in basalts from DSDP Legs 45 and 46: evidence for magma mixing. *Contributions to Mineralogy and Petrology* **67**, 417–431.

Eason, D. & Sinton, J. (2006). Origin of high-Al N-MORB by fractional crystallization in the upper mantle beneath the Galapagos Spreading Center. *Earth and Planetary Science Letters* **252(3–4)**, 423–436.

Fowler, C. M. R. (2008). *The Solid Earth: An Introduction to Global Geophysics*. Cambridge: Cambridge University Press.

Frey, F. A., Suen, C. J. & Stockman, H. W. (1985). The Ronda high temperature peridotite: geochemistry and petrogenesis. *Geochimica et Cosmochimica Acta* **49**, 2469–2491.

Gale, A., Escrig, S., Gier, E. J., Langmuir, C. H. & Goldstein, S. L. (2011). Enriched basalts at segment centers: The Lucky Strike (37°17′N) and Menez Gwen (37°50′N) segments of the Mid-Atlantic Ridge. *Geochemistry, Geophysics, Geosystems* **12**, Q06016, doi:10.1029/2010GC003446.

Gale, A., Dalton, C. A., Langmuir, C. H., Su, Y. & Schilling, J.-G. (2013*a*). The mean composition of ocean ridge basalts. *Geochemistry, Geophysics, Geosystems* **14**, 489–518, doi:10.1029/2012GC004334.

Gale, A., Laubier, M., Escrig, S. & Langmuir, C. H. (2013*b*). Constraints on melting processes and plume–ridge interaction from comprehensive study of the FAMOUS and North Famous Segments, Mid-Atlantic Ridge. *Earth and Planetary Science Letters* **365**, 209–220.

Ghiorso, M. S., Hirschmann, M. M., Reiners, P. W. & Kress, V. C. (2002). The pMELTS: A revision of MELTS for improved calculation of phase relations and major element partitioning related to partial melting of the mantle to 3 GPa. *Geochemistry, Geophysics, Geosystems* **3**, doi:10.1029/2001GC000217.

Green, D. H., Falloon, T. J., Eggins, S. M. & Yaxley, G. M. (2001). Primary magmas and mantle temperatures. *European Journal of Mineralogy* **13(3)**, 437–451.

Grove, T. L., Kinzler, R. J. & Bryan, W. B. (1992). Fractionation of mid-ocean ridge basalt (MORB). Mantle flow and melt generation at mid-ocean ridges. In: Phipps Morgan, J., Blackman, D. K. & Sinton, J. M. (eds) *Mantle Flow and Melt Generation at Mid-Ocean Ridges. American Geophysical Union, Geophysical Monograph* **71**, 281–310.

Halliday, A. N., Lee, D. C., Tommasini, S., Davies, G. R., Paslick, C. R., Fitton, J. G. & James, D. E. (1995). Incompatible trace elements in OIB and MORB and source enrichment in the sub-oceanic mantle. *Earth and Planetary Science Letters* **133(3–4)**, 379–395.

Hanson, G. & Langmuir, C. H. (1978). Modeling of major elements in mantle-melt systems using trace element approaches. *Geochimica et Cosmochimica Acta* **42**, 725–742.

Hirose, K. & Kushiro, I. (1993). Partial melting of dry peridotites at high pressures: determination of compositions of melts segregated from peridotite using aggregates of diamond. *Earth and Planetary Science Letters* **114**, 477–489.

Hirschmann, M. M., Baker, M. B. & Stolper, E. M. (1998). The effect of alkalis on the silica content of mantle-derived melts. *Geochimica et Cosmochimica Acta* **62**, 883–902.

Katsura, T. (1995). Thermal-diffusivity of olivine under upper-mantle conditions. *Geophysical Journal International* **122(1)**, 63–69.

Katz, R. F., Spiegelman, M. & Langmuir, C. H. (2003). A new parameterization of hydrous mantle melting. *Geochemistry, Geophysics, Geosystems* **4**, doi:10.1029/2002GC000433.

Kelley, K. A., Plank, T., Grove, T. L., Stolper, E. M., Newman, S. & Hauri, E. H. (2006). Mantle melting as a function of water content beneath back-arc basins. *Journal of Geophysical Research* **111(B09208)**, doi:10.1029/2005JB003732.

Kimura, J.-I. & Sano, S. (2012). Reactive melt flow as the origin of residual mantle lithologies and basalt chemistries in mid-ocean ridges: implications from the Red Hills peridotite, New Zealand. *Journal of Petrology* **53**, 1637–1671.

Kinzler, R. J. (1997). Melting of mantle peridotite at pressures approaching the spinel to garnet transition: Application to mid-ocean ridge basalt petrogenesis. *Journal of Geophysical Research* **102(B1)**, 853–874, doi:10.1029/96JB00988.

Klein, E. M. & Langmuir, C. H. (1987). Global correlations of ocean ridge basalt chemistry with axial depth and crustal thickness. *Journal of Geophysical Research* **92(B8)**, 8089–8115.

Klein, E. M. & Langmuir, C. H. (1989). Local versus global variations in ocean ridge basalt composition: A reply. *Journal of Geophysical Research* **94**, 4241–4252.

Langmuir, C. H. (1989). Geochemical consequences of *in situ* crystallization. *Nature* **340**, 199–205.

Langmuir, C. & Bender, J. (1984). Geochemical variations around transform faults: observations and implications. *Earth and Planetary Science Letters* **69**, 107–127.

Langmuir, C. H. & Hanson, G. N. (1980). An evaluation of major element heterogeneity in the mantle sources of basalts. *Philosophical Transactions of the Royal Society of London, Series A* **297(1431)**, 383–407.

Langmuir, C. H., Bender, J. F., Bence, A. E., Hanson, G. N. & Taylor, S. R. (1977). Petrogenesis of basalts from the FAMOUS area: Mid-Atlantic Ridge. *Earth and Planetary Science Letters* **36**, 133–156.

Langmuir, C. H., Klein, E. M. & Plank, T. (1992). Petrological systematics of midocean ridge basalts—Constraints on melt generation beneath ocean ridges. In: Phipps Morgan, J., Blackman, D. K. & Sinton, J. M. (eds) *Mantle Flow and Melt*

Generation at Mid-Ocean Ridges. American Geophysical Union, Geophysical Monograph **71**, 183–280.

Langmuir, C. H., Bezos, A., Escrig, S. & Parman, S. W. (2006). Chemical systematics and hydrous melting of the mantle in back-arc basins. In: Christie, D. M., Fisher, D. M., Lee, S.-M. *et al.* (eds) *Back-Arc Spreading Systems: Geological, Biological, Chemical and Physical Interactions. American Geophysical Union*, doi:10.1029/166GM07.

Laubier, M. L., Gale, A. & Langmuir, C. H. (2012). Melting and crustal processes at the FAMOUS segment (Mid-Atlantic Ridge): new insights from olivine-hosted melt inclusions from multiple samples. *Journal of Petrology* **53(4)**, 665–698.

Lehnert, K., Su, Y., Langmuir, C. H., Sarbas, B. & Nohl, U. (2000). A global geochemical database structure for rocks. *Geochemistry, Geophysics, Geosystems* **1**, 1012.

McKenzie, D. & O'Nions, R. K. (1995). The source regions of ocean island basalts. *Journal of Petrology* **36(1)**, 133–159.

Melson, W. G. & O'Hearn, T. (1979). Basaltic glasses erupted along the Mid-Atlantic Ridge between 0–37°N latitude: correlations between composition and latitude. In: Talwani, M., Harrison, C. G., Hayes, D. E. *et al.* (eds) *Deep Drilling Results in the Atlantic Ocean: Ocean Crust. American Geophysical Union*, doi:10.1029/2011JB009044.

Niu, Y. & Batiza, R. (1994). Magmatic processes at a slow spreading ridge segment: 26°S Mid-Atlantic Ridge. *Journal of Geophysical Research* **99(B10)**, 19719–19740, doi:10.1029/94JB01663.

Niu, Y. L. & O'Hara, M. J. (2008). Global correlations of ocean ridge basalt chemistry with axial depth: A new perspective. *Journal of Petrology* **49(4)**, 633–664.

Niu, Y. L., Collerson, K. D., Batiza, R., Wendt, J. I. & Regelous, M. (1999). Origin of enriched-type mid-ocean ridge basalt at ridges far from mantle plumes: The East Pacific Rise at 11°20′N. *Journal of Geophysical Research—Solid Earth* **104(B4)**, 7067–7087.

O'Hara, M. J. (1977). Geochemical evolution during fractional crystallisation of a periodically refilled magma chamber. *Nature* **266**, 503–507.

O'Neill, H. S. C. & Jenner, F. E. (2012). The global pattern of trace-element distributions in ocean floor basalts. *Nature* **491(7426)**, 698–704.

Plank, T. & Langmuir, C. H. (1993). Tracing trace elements from sediment input to volcanic output at subduction zones. *Nature* **362**, 739–742.

Presnall, D. C., Gudfinnsson, G. H. & Walter, M. J. (2002). Generation of mid-ocean ridge basalts at pressures from 1 to 7 GPa. *Geochimica et Cosmochimica Acta* **66(12)**, 2073–2090.

Reid, I. & Jackson, R. (1981). Oceanic spreading rate and crustal thickness. *Marine Geophysical Researches* **5**, 165–172.

Roeder, P. L. & Emslie, R. F. (1970). Olivine–liquid equilibrium. *Contributions to Mineralogy and Petrology* **29**, 275–289.

Rubin, K. H. & Sinton, J. M. (2007). Inferences on mid-ocean ridge thermal and magmatic structure from MORB compositions. *Earth and Planetary Science Letters* **260(1–2)**, 257–276, doi:10.1016/j.epsl.2007.05.035.

Rudge, J. F., McKenzie, D. & Haynes, P. H. (2005). A theoretical approach to understanding the isotopic heterogeneity of mid-ocean ridge basalt. *Geochimica et Cosmochimica Acta* **69(15)**, 3873–3887.

Ryan, W. B. F. *et al.* (2009). Global multi-resolution topography synthesis. *Geochemistry, Geophysics, Geosystems* **10**, Q03014, doi:10.1029/2008GC002332.

Salters, V. J. M. & Stracke, A. (2004). Composition of the depleted mantle. *Geochemistry, Geophysics, Geosystems* **5(5)**, 27.

Schilling, J. G. (1975). Azores mantle blob—rare-Earth evidence. *Earth and Planetary Science Letters* **25(2)**, 103–111.

Schilling, J. G., Bergeron, M. B. & Evans, R. (1980). Halogens in the mantle beneath the North Atlantic. *Philosophical Transactions of the Royal Society of London, Series A* **297(1431)**, 147–178.

Schwab, B. E. & Johnston, A. D. (2001). Melting systematics of modally variable, compositionally intermediate peridotites and the effects of mineral fertility. *Journal of Petrology* **42(10)**, 1789–1811.

Shen, Y. & Forsyth, D. W. (1995). Geochemical constraints on initial and final depths of melting beneath midocean ridges. *Journal of Geophysical Research—Solid Earth* **100(B2)**, 2211–2237.

Shorttle, O. & Maclennan, J. (2011). Compositional trends of Icelandic basalts: Implications for short length-scale lithological heterogeneity in mantle plumes. *Geochemistry, Geophysics, Geosystems* **12**, Q11008.

Sobolev, A. V., Hofmann, A. W., Jochum, K. P., Kuzmin, D. V. & Stoll, B. (2011). A young source for the Hawaiian plume. *Nature* **476(7361)**, 434–437.

Stolper, E. & Newman, S. (1994). The role of water in the petrogenesis of Mariana trough magmas. *Earth and Planetary Science Letters* **121**, 293–325.

Sun, S. S. & McDonough, W. F. (1989). Chemical and isotopic systematics of oceanic basalts: Implications for mantle composition and processes. In: Saunders, A. D. & Norry, M. J. (eds) *Magmatism in the Ocean Basins. Geological Society, London, Special Publications* **42**, 313–345.

Taylor, B. & Martinez, F. (2003). Back-arc basin basalt systematics. *Earth and Planetary Science Letters* **210**, 481–497.

Till, C. B., Grove, T. L. & Krawczynski, M. J. (2012). A melting model for variably depleted and enriched lherzolite in the plagioclase and spinel stability fields. *Journal of Geophysical Research—Solid Earth* **117**, doi:10.1029/2011JB009044.

Tormey, D. R., Grove, T. L. & Bryan, W. B. (1987). Experimental petrology of normal MORB near the Kane Fracture Zone: 22°–25°N, Mid-Atlantic Ridge. *Contributions to Mineralogy and Petrology* **96**, 121–139.

Wasylenki, L. E., Baker, M. B., Kent, A. J. R. & Stolper, E. M. (2003). Near-solidus melting of the shallow upper mantle: partial melting experiments on depleted peridotite. *Journal of Petrology* **44(7)**, 1163–1191.

Weaver, J. & Langmuir, C. H. (1990). Calculation of phase equilibrium in mineral–melt systems. *Computers and Geosciences* **16**, 1–19.

White, W. M. & Bryan, W. B. (1977). Sr-isotope, K, Rb, Cs, Sr, Ba, and rare-earth geochemistry of basalts from the FAMOUS area. *Geological Society of America Bulletin* **88**, 571–576.

Winpenny, B. & Maclennan, J. (2011). A partial record of mixing of mantle melts preserved in Icelandic phenocrysts. *Journal of Petrology* **52**, 1791–1812.

Workman, R. K. & Hart, S. B. (2005). Major and trace element composition of the depleted MORB mantle (DMM). *Earth and Planetary Science Letters* **231**, 53–72.

Yang, H.-J., Kinzler, R. J. & Grove, T. L. (1996). Experiments and models of anhydrous, basaltic olivine–plagioclase–augite saturated melts from 0·001 to 10 kbar. *Contributions to Mineralogy and Petrology* **124**, 1–18.

Zhou, H. Y. & Dick, H. J. B. (2013). Thin crust as evidence for depleted mantle supporting the Marion Rise. *Nature* **494(7436)**, 195–200.